



Targeting PKLR/MYCN/ROMO1 signaling suppresses neuroendocrine differentiation of castration-resistant prostate cancer

Wei-Yu Chen^{a,b,1}, Phan Vu Thuy Dung^{c,1}, Hsiu-Lien Yeh^c, Wei-Hao Chen^c, Kuo-Ching Jiang^c, Han-Ru Li^c, Zi-Qing Chen^d, Michael Hsiao^e, Jiaoti Huang^f, Yu-Ching Wen^{g,h,i,**}, Yen-Nien Liu^{c,j,*}

^a Department of Pathology, Wan Fang Hospital, Taipei Medical University, Taipei, Taiwan

^b Department of Pathology, School of Medicine, College of Medicine, Taipei Medical University, Taipei, Taiwan

^c Graduate Institute of Cancer Biology and Drug Discovery, College of Medical Science and Technology, Taipei Medical University, Taipei, Taiwan

^d Division of Clinical Pharmacy, School of Pharmacy, Taipei Medical University, Taipei, Taiwan

^e Genomics Research Center, Academia Sinica, Taipei, Taiwan

^f Department of Pathology, Duke University Medical Center, Durham, NC, USA

^g Department of Urology, Wan Fang Hospital, Taipei Medical University, Taipei, Taiwan

^h Department of Urology, School of Medicine, College of Medicine, Taipei Medical University, Taipei, Taiwan

ⁱ TMU Research Center of Urology and Kidney, Taipei Medical University, Taipei, Taiwan

^j TMU Research Center of Cancer Translational Medicine, Taipei Medical University, Taipei, Taiwan

ARTICLE INFO

Keywords:

Androgen deprivation therapy (ADT)
Neuroendocrine prostate cancer (NEPC)
Pyruvate kinase L/R (PKLR)
Reactive oxygen species modulator 1 (ROMO1)
MYCN proto-oncogene (MYCN)

ABSTRACT

Conventional treatment of prostate cancer (PCa) uses androgen-deprivation therapy (ADT) to inhibit androgen receptor (AR) signaling-driven tumor progression. ADT-induced PCa recurrence may progress to an AR-negative phenotype with neuroendocrine (NE) histologic features, which are associated with metabolic disturbances and poor prognoses. However, the metabolic pathways that regulate NE differentiation (NED) in PCa remain unclear. Herein, we show a regulatory mechanism in NED-associated metabolism dysfunction induced by ADT, whereby overexpression of pyruvate kinase L/R (PKLR) mediates oxidative stress through upregulation of reactive oxygen species modulator 1 (ROMO1), thereby promoting NED and aggressiveness. ADT mediates the nuclear translocation of PKLR, which binds to the MYCN/MAX complex to upregulate *ROMO1* and NE-related genes, leading to altered mitochondrial function and NED of PCa. Targeting nuclear PKLR/MYCN using bromodomain and extra-terminal motif (BET) inhibitors has the potential to reduce PKLR/MYCN-driven NED. Abundant ROMO1 in serum samples may provide prognostic information in patients with ADT. Our results suggest that ADT resistance leads to upregulation of PKLR/MYCN/ROMO1 signaling, which may drive metabolic reprogramming and NED in PCa. We further show that increased abundance of serum ROMO1 may be associated with the development of NE-like PCa.

1. Introduction

Prostate cancer (PCa) is a common health problem with an increasing annual incidence in men worldwide [1]. As androgen receptor (AR) signaling plays an important role in the occurrence and development of PCa, clinical targeting of the AR signaling cascade by androgen-deprivation therapy (ADT) has achieved great success [2]. However, many cases of PCa develop into castration-resistant PCa

(CRPC), which is more aggressive and refractory to therapy [3,4]. Treatment of CRPC with more-effective AR-targeted therapies such as enzalutamide/MDV3100 and abiraterone may lead to an increase in AR low/negative (AR^{low/-}) CRPC subtypes [3,4]. AR-targeted therapy can be used to treat AR-positive CRPC; however, there are limited therapeutic options for AR^{low/-} CRPC [5]. Histologically, the main subset of AR^{low/-} CRPC is neuroendocrine (NE) PCa (NEPC), which is characterized by the loss of AR expression and increased expression of NE markers such as

* Corresponding author. Taipei Medical University, 250 Wu-Hsing Street, Taipei, 11031, Taiwan.

** Corresponding author. Taipei Medical University, 250 Wu-Hsing Street, Taipei, 11031, Taiwan.

E-mail addresses: 95207@w.tmu.edu.tw (Y.-C. Wen), liuy@tmu.edu.tw (Y.-N. Liu).

¹ These authors contributed equally to this work.

chromogranin A (*CHGA*), synaptophysin (*SYP*), neuron-specific enolase (*ENO2*), and MYCN proto-oncogene (*MYCN*) [6]. The trans-differentiation of AR-positive CRPC to NEPC is driven by different signaling molecules. Depletion of AR signaling was shown to be associated with induction of epithelial-to-mesenchymal transition (EMT) signaling in PCa cells and appears to drive tumor aggressiveness in NEPC [7,8]. Hypoxia-mediated Notch signaling downregulation and RE1 silencing transcription factor (REST) repression result in overexpression of neural genes (*CHGA*, *SYP*, and *AURKA*) and promote the NE-phenotype [9,10]. However, the metabolomic effectors driving NE differentiation (NED) and the development of more-aggressive small-cell PCa (SCPC) remain largely unknown.

Cancer cells have a high glycolytic and mitochondrial propensity to support nutrient depletion [11]. Alterations in mitochondrial (mt)DNA and the mitochondrial membrane potential (MMP) frequently occur in cancer cells, leading to altered mitochondrial function and reactive oxygen species (ROS) production [12]. ROS-mediated regulation of oncogenic signaling can cause oxidative damage, which further affects tumorigenesis and metastasis [13]. Increased ROS levels drive cells to enter a state of hyperproliferation accompanied by DNA damage, which further enhances drug resistance [13]. ROS were shown to activate resistance to multiple chemotherapeutic agents in various cancers, including PCa [14,15]. Dysregulation of AR signaling increases intracellular ROS levels [16]. Upregulation of ROS levels promotes the aggressive phenotype of PCa cells through increased ROS production and metabolic reprogramming [13]. The increase in metabolic reprogramming can support cell proliferation and lead to epigenetic changes, thereby promoting the development of NED subtypes of PCa [17]. However, the mechanism underlying ROS upregulation caused by ADT-induced metabolic enzymes that promotes mitochondrial biogenesis and which acts as a tumor promoter in the NED progression of PCa is currently unclear.

In metabolic reprogramming, glycolytic enzymes such as pyruvate kinase were found to be involved in regulating the development of CRPC and NEPC [18]. Pyruvate kinase irreversibly catalyzes the *trans*-phosphorylation between phosphoenolpyruvate (PEP) and adenosine diphosphate (ADP), generating pyruvate and adenosine triphosphate (ATP) [19]. Among the four isoenzymes of pyruvate kinase, the L and R isoenzymes are expressed by the pyruvate kinase L/R (*PKLR*) gene, while the M1 and M2 isoenzymes are expressed by the pyruvate kinase isoenzyme M2 (*PKM2*) gene. PKM2 is expressed in tissues with anabolic functions, promotes cell proliferation, and is subjected to complex allosteric regulation [20]. PKM2 can be translocated into the nucleus through activation of the epidermal growth factor receptor (EGFR) [21] or hypoxic [22] pathways. Whether PKLR is translocated into the nucleus during disease progression remains unknown. PKLR is required to maintain levels of the major endogenous antioxidant, glutathione, and is important for colorectal cancer cell survival in the tumor core [23]. PKLR acts as a regulator of lipid metabolism and mitochondrial function by promoting mitochondrial function in liver and kidney cells [24,25]. Our recent findings suggest that PKLR is upregulated by loss of androgen-responsive transcription factor, zinc finger and BTB domain containing 10 (*ZBTB10*) that regulates glucose metabolism and promotes NED of PCa after ADT [26]. However, the role of PKLR in mediating mitochondrial function to promote therapeutic resistance and NED in PCa remains unclear.

Since upregulated mitochondrial biogenesis and mtDNA contents after ADT were found to be related to metabolic disorders that lead to therapeutic resistance in PCa [27–29], we sought to determine signal transduction profiles that characterize upregulation of PKLR-driven metabolic reprogramming and their effects on the progression of ADT-resistant or NE-like PCa. Abnormalities in ROS sensors cause an imbalance in active oxygen regulators in PCa [30]. We found that ADT induced PKLR overexpression, which may be related to upregulation of the ROS sensor, ROS modulator 1 (*ROMO1*). *ROMO1* has two α -helices located in the inner mitochondrial membrane [31], where its

homohexamer forms a viroporin-like cation channel that plays a major role in balancing the mitochondrial reduction-oxidation state [32]. We show that PKLR overexpression upregulated *ROMO1* and enhanced mitochondrial function; however, *ROMO1*-knockdown (KD) reduced oxidative stress in PCa cells. Interestingly, PKLR may be translocated to the nucleus after ADT, where it acts as a transcription factor, possibly by interacting with the nuclear MYCN/MAX complex and upregulating *ROMO1* and NE markers, resulting in altered mitochondrial function and NED in PCa cells. Our study links two molecular mechanisms whereby low AR output is associated with increased abundance of the nuclear PKLR/MYCN/MAX complex in PCa, which upregulates *ROMO1*-driven altered mitochondrial function and enhances NE marker expression.

2. Materials and methods

2.1. Cell lines, reagents, and constructs

The VCaP, LNCaP, C4-2, and PC3 PCa cell lines were purchased from ATCC (Manassas, VA, USA). All cells were cultured in RPMI 1640 medium supplemented with 10% fetal bovine serum (FBS). The LASCPC01 NEPC-like cell line was purchased from ATCC and cultured in RPMI 1640 medium supplemented with 0.005 mg/ml insulin (Sigma-Aldrich), 0.01 mg/ml transferrin (Sigma-Aldrich), 30 nM sodium selenite (Sigma-Aldrich), 10 nM hydrocortisone (Sigma-Aldrich), 10 nM β -estradiol (Sigma-Aldrich), 4 mM L-glutamine (Invitrogen), and 5% FBS. LNCaP/Tet-PKLR cells were generated by stably transfecting LNCaP cells with a Tet-PKLR-inducible lentiviral vector (pInducer20, #44012; Addgene). PKLR was induced by treatment with 25 ng of doxycycline (Dox, Med-ChemExpress) for 24 h. The MDV3100-resistant cell line, C4-2-MDVR, is a viable cell line generated by growing C4-2 cells under selection pressure of 30 μ M MDV3100 (enzalutamide, Selleck Chemicals) for 6 months in 10% FBS-containing medium. Cells in the medium were cultured at 37 °C with 5% CO₂ and saturated humidity, and all cell lines routinely tested negative for mycoplasma contamination. To mimic ADT, LNCaP cells were cultured in complete medium containing 5% charcoal-stripped serum (CSS, ThermoFisher) for 1–3 weeks. Rescue ADT was administered as 10 nM dihydrotestosterone (DHT; Sigma-Aldrich) 24 h after week 3 of ADT. For MYCN inhibitor treatment, LNCaP, C4-2, C4-2-MDVR, or PC3 cells were treated with 30 μ M of the bromodomain and extraterminal motif (BET) inhibitor (JQ1 [33] or OTX-15 [34], Sigma-Aldrich) for 24 h. The non-target control (NC), PKLR-KD, or *ROMO1*-KD using Luciferase (*Luc*), PKLR, or *ROMO1* small hairpin (*sh*) RNA vector (pKLO.1) were obtained from the RNAi Core Laboratory (Academic Sinica, Taipei, Taiwan). Small interfering (si)RNAs (NC, siMYC, and siMYCN) were obtained from ON-TARGETplus SMARTpool siRNAs (D-001810-10, L-003282-02, and L-003913-01; Horizon Discovery). A stably expressing empty vector (EV), PKLR, or *ROMO1* in cells was generated by respectively transfecting pCDH-CMV-MCS-EF1-Puro, pCDH-CMV-PKLR-EF1-Puro, or pCDH-CMV-*ROMO1*-EF1-Puro vectors (CD510B-1; System Biosciences) and selected with 1 μ g/ml puromycin (ThermoFisher) for 1 month.

2.2. Reverse-transcription quantitative polymerase chain reaction (RT-qPCR) analysis

An RNA isolation kit (Qiagen) was used for total messenger (m)RNA isolation. Three micrograms of total mRNA was used for RT using a SuperScript III kit (Invitrogen). PCR amplification used SYBR Green PCR master mix (Applied Biosystems) with a thermocycler run for an initial 95 °C incubation for 10 min, followed by 40 cycles of 95 °C for 15 s and 60 °C for 1 min. Thresholds were normalized to the expression of the internal control, human 18S ribosomal (r)RNA, and run in triplicate. mRNA levels were quantified using the comparative Ct method. Experiments were performed using a StepOnePlus real-time PCR system (Applied Biosystems), and data were processed using ABI SDS ver. 2.1

software (Applied Biosystems). All primers used for the PCR are listed in [Supplementary Table S2](#).

2.3. mtDNA extraction and analysis

mtDNA was extracted using a QIAamp® DNA isolation kit (Qiagen). Briefly, 3×10^6 cells were harvested and mixed with 200 μ L lysis buffer (buffer ATL, Qiagen) and proteinase K (Roche). The mixture was prepared according to the protocol described in the users' manual. The quantity of mtDNA was determined using a real-time qPCR as previously described [35]. PCR cycles used for mtDNA detection were as follows: 2 min at 50 °C, 10 min at 95 °C, and 40 cycles at 95 °C for 15 s and 60 °C for 60 s. Primer sequences for Haplogroup M18 mtDNA and 18S RNA nuclear (n)DNA copy number detection were as follows: mtDNA_F: CGCCTCACACTCATTCTCAACC; mtDNA_R: CAAGGAAGGGGTAGGC-TATGTG; nDNA_F: AGTCCCCACAACACTGAGA; and nDNA_R: AATGGCACAGACAAGGTGG. The relative quantity of mtDNA was normalized using the following formula: $\text{mtDNA} = 2^{-(\text{C}_{\text{mtDNA}} - \text{C}_{\text{nDNA}})}$, where C_{mtDNA} and C_{nDNA} respectively refer to threshold cycles of Haplogroup M18 mtDNA and 18S RNA nDNA.

2.4. Colorimetric ATP assay

A colorimetric ATP assay was performed using an ATP assay kit (Abcam) according to the manufacturer's protocol, with some modifications. Briefly, 10^6 cells were harvested and lysed with an ATP assay buffer. Cells in the reaction mixture were lysed and incubated for 30 min at room temperature. The optical density (OD) at 570 nm was measured using a CLARIOstar microplate reader (BioTek), and the amount (μ M) of ATP was calculated by referring to a calibration curve.

2.5. Oxygen consumption rate (OCR) analysis

OCR measurements using a mitochondrial stress assay kit (Seahorse Bioscience) were performed with a Seahorse XF24 extracellular flux analyzer (Seahorse Bioscience). In total, 5×10^4 cells/well of desired cells were inoculated into a Seahorse analyzer-specific culture plate (Seahorse Bioscience) and incubated overnight. A mitochondrial stress test was used to obtain bioenergetic parameters in cells following the sequential addition of inhibitors of mitochondrial function: 1 μ M oligomycin, 0.75 μ M carbonyl cyanide-*p*-trifluoromethoxyphenylhydrazone (FCCP), and a combination of rotenone and antimycin A (at 0.5 μ M each).

2.6. Cellular ROS analysis

A 2',6'-dichlorofluorescein diacetate (DCFDA) cellular ROS assay kit (Abcam) was used to quantify ROS levels. All steps were performed based on the manufacturer's protocol. In brief, 2×10^4 cells were harvested and incubated with 25 μ M DCFDA for 30 min at 37 °C. After incubation, excess dye was washed out with 1 \times Buffer solution, followed by a fluorescence-activated cell sorting (FACS) analysis (BD Biosciences) with excitation/emission wavelengths at 485 nm/535 nm. Forward and side scatter gates were established to remove cell debris and cellular aggregates; 10^4 live cell events were then recorded and analyzed using FACSDiva software (BD Biosciences) and normalized to the value of the vehicle.

2.7. Proliferation assay

Cell viability was analyzed by staining cells with a crystal violet fixative solution (Sigma-Aldrich). For the experiment, a density of 500 cells/well were seeded in multiple wells of 96-well plates. Proliferation rates were assessed every 24 h for seven days. Each day, one plate was stained with a 0.5% crystal violet fixative solution for 15 min, rinsed

three times with distilled water, and allowed to air-dry. At the end of the experiment, the crystal violet was dissolved by adding 100 μ L of 50% ethanol containing 0.1 M sodium citrate to each well. The absorbance was quantified at a wavelength of 540 nm using a CLARIOstar microplate reader (BioTek). Relative cell numbers are presented as a ratio of OD 540 nm normalized to day 0.

2.8. Three-dimensional (3D) sphere-formation assay

For the sphere-formation assay, a single-cell suspension of 1000 cells/well in cold Matrigel™ (Corning) was mixed at a 1:1 ratio with serum-free medium. Cells were uniformly seeded in a circular manner around the bottom rim of the wells in a 24-well plate and cultured in a 37 °C incubator for 45 min to solidify the Matrigel. Spheres were replenished with warm complete medium, as in the original seeding, every 2 days at 37 °C in a humidified incubator for 6 days. Tumor spheres in each well were observed, and a snapshot was taken with a phase-contrast microscope (Olympus) and counted in three independent experiments with triplicate samples.

2.9. Invasion and migration assays

For the invasion assay, Matrigel-coated Transwell dishes were prepared by adding 200 μ L of CSS-containing medium diluted with Matrigel. Three thousand cells were resuspended in 600 μ L of serum-free medium and added to Matrigel-coated 24-well Transwell dishes. The lower chamber was filled with 600 μ L of 10% FBS-containing medium. After 12 h, cells that had invaded the Matrigel-coated Transwell were fixed and stained with 0.5% crystal violet for 15 min. A phase-contrast microscope (Olympus) was used to capture a snapshot of the invading cells under the membrane, and three replicates were counted each time. The migration assay was performed using transwells without Matrigel, and cells were fixed and stained as described for the invasion assay.

2.10. Western blot (WB) analysis

Briefly, 2×10^6 cells were harvested by lysis in 100 μ L of RIPA buffer (Bio-Rad) containing complete protease inhibitors (Roche) and phosphatase inhibitors (Roche). Protein concentrations in the lysed fractions were quantified using the Bradford reagent (Bio-Rad), and 30 μ g of protein was used for the WB analysis. After transfer to polyvinylidene difluoride (PVDF) or nitrocellulose membranes (Merck Millipore), blots were blocked with 5% bovine serum albumin (BSA) in 0.1% Tween-20 in phosphate-buffered saline (PBST/PBS). Primary antibodies were incubated overnight at 4 °C, and secondary antibodies were incubated at room temperature for 1 h, as indicated in [Supplementary Table S3](#). The protein intensity was measured by ImageJ software (National Institutes of Health), and three independent experiments were performed.

2.11. Mitochondrial membrane potential (MMP) analysis

For MMP detection, 10^6 cells/well were seeded into 10-cm culture dishes, harvested after 24 h, washed twice with warm PBS, and stained with 50 nM 3,3'-diethyloxycarbocyanine iodide (DiOC₂(3), Sigma-Aldrich)/PBS while being protected from light at 37 °C for 1 h. After staining, cells were washed once with warm PBS, and the fluorescence intensity was measured using a Canto II flow cytometer (BD Biosciences). A fluorescent detector for MMP detection used the B/E channel (488 nm excitation and 670 nm long-pass emission). B/E channel data from the MMP assay were plotted as a dot plot and gated by the 2 μ M carbonyl cyanide 3-chlorophenylhydrazone (CCCP, Sigma-Aldrich)-treated group. Values of the relative median fluorescence intensity (MFI) of DiOC₂(3) were measured by FACS (BD Biosciences) using FACSDiva software (BD Biosciences) and normalized to the value of the vehicle. Three independent experiments were performed in triplicate.

2.12. Tumorigenicity assays in mice

Animal experiments were performed in accordance with a protocol (no.: LAC-2021-0444) approved by the Taipei Medical University Animal Care and Use Committee. For the tumorigenicity assays, 6-week-old male nude mice (obtained from the NLAC, Taipei, Taiwan) were randomly divided into four groups of five mice each and subcutaneously injected with 2.5×10^6 LNCaP/Tet-PKLR cells with the control vector or ROMO1 shRNA vector in 50% Matrigel (Corning). Four weeks after the injection, Dox-treated mice were administered Dox at a concentration of 2 mg/ml in drinking water for 10 weeks under double-blind conditions. For MYCN inhibitor treatment, ten mice per group (DMSO and JQ1) were subcutaneously injected with 3.5×10^5 LASCPC01 cells, and mice were intraperitoneally treated with DMSO or JQ1 (30 mg/kg body weight) twice a week for 6 weeks under double-blind conditions. Tumor sizes were measured weekly using calipers, and the tumor volume was calculated using the following formula: tumor volume = $(4/3) \times (L/2) (W/2)^2$, where L is the length and W is the width. The results are presented as the mean \pm standard error (SE) for each experimental group.

2.13. Immunohistochemical (IHC) staining

The tissue microarray (TMA) set, which included 40 cases of prostatic carcinoma and 10 cases of benign prostatic tissue, was purchased from SuperBioChips Laboratories (#CA4). Tumor samples from 17 PCa patients before and after ADT were collected from Taipei Medical University-Wan Fang Hospital (Taipei, Taiwan), and the study protocol was approved by the Taipei Medical University Joint Institutional Review Board (approval no. N202201057). Treatment information for PCa patients before and after ADT is shown in Supplemental file 3. Sections were deparaffinized, rehydrated, and blocked with 3% hydrogen peroxide. Heat-induced antigen retrieval was performed in citric acid buffer (pH 6.0) at 121 °C for 10 min in a decloaking chamber (Biocare Medical). Sections were incubated with a diluted primary antibody at room temperature for 2 h. Antibodies used for IHC are listed in [Supplementary Table S4](#). Sections were then incubated with a biotin-conjugated secondary antibody (Biocare Medical) at room temperature for 20 min, followed by incubation with a prediluted streptavidin-horseradish peroxidase complex at room temperature for 20 min. Immunoreactivity was revealed by adding 3,3'-diaminobenzidine, followed by hematoxylin staining. Pathological diagnoses and Gleason grading of these cases were confirmed microscopically by a pathologist (Wei-Yu Chen). The intensities of nuclear PKLR and cytoplasmic ROMO1 staining were scored semiquantitatively as negative, weakly positive, moderately positive, and strongly positive. Correlations of the grading of prostatic adenocarcinomas with ROMO1 expression were compared using a Chi-squared test in SPSS statistical 18.0 software (SPSS). For the relative intensity of nuclear PKLR and its correlation with cytoplasmic ROMO1 in PCa patients before and after ADT, significance was determined using a one-way analysis of variance (ANOVA) in GraphPad Prism (GraphPad Software).

2.14. Immunoprecipitation (IP)-WB analysis

The IP-WB assay was performed using a Pierce™ classic magnetic IP/CO-IP kit (ThermoFisher). For IP, 2×10^7 LASCPC01 or C4-2-MDVR cells were treated with DMSO, 30 μ M JQ1 or 30 μ M OTX-15 for 24 h, and then lysed with IP buffer (0.025 M Tris-HCl (pH 7.4), 0.15 M NaCl, 0.001 M EDTA, 1% NP40, 5% glycerol, and 1% protease inhibitor cocktail) for 15 min on ice, followed by centrifugation at $1.3 \times 10^4 \times g$ for 10 min at 4 °C. Subsequently, 500 μ g of the protein supernatant was incubated with 5 μ g of PKLR (sc-133224; Santa Cruz Biotechnology), an MYCN antibody (sc-53993; Santa Cruz Biotechnology), or control immunoglobulin G (IgG) overnight at 4 °C. Protein A/G magnetic beads were then added and incubated for 1 h with shaking at room temperature. After washing the beads thrice with IP buffer, the immune complex

was collected on ice and subjected to a WB analysis. Antibodies used for WB are listed in [Supplementary Table S3](#).

2.15. Chromatin IP (ChIP) assay

ChIP assays were performed using an EZ Magna ChIP A kit (Merck Millipore), according to a modified protocol. ADT-treated LNCaP, C4-2-MDVR, or LASCPC01 cells were treated with 30 μ M JQ1 or 30 μ M OTX-15 for 24 h, and then crosslinked with 1% formaldehyde in culture medium at room temperature for 15 min, followed by the addition of 1 ml $10 \times$ glycine treatment. Cells were washed twice with cold PBS containing a protease inhibitor (Roche) and centrifuged at 10^5 rpm. Cell pellets were resuspended in cell lysis buffer (0.5 mL) and incubated on ice for 15 min. Nuclei were collected by centrifugation at 10^5 rpm and 4 °C for 10 min and resuspended in nuclear lysis buffer. Genomic DNA was sheared with a microtip during sonication (Branson Sonifier 250, Emerson) following 15 cycles of a 20-s burst then 1 min on ice. This procedure resulted in DNA fragments of approximately 100–300 bp in length. Sheared chromatin was aliquoted to perform IP with the indicated antibodies at 4 °C overnight. A qPCR was performed in triplicate with 2 μ l of eluted chromatin. ChIP antibodies and PCR primers used are listed in [Supplementary Table S5](#). For the ChIP-sequencing (Seq) analysis, ChIP-Seq data were downloaded from the Gene Expression Omnibus (GEO) (GSM2915909_MYCN and GSM1711858_MAX) and analyzed with the Genome Browser (Genomics Institute, University of California at Santa Cruz, Santa Cruz, CA, USA).

2.16. Promoter reporter assay

For the promoter reporter assays, 5×10^4 cells/well of C4-2-MDVR-, LASCPC01-, or CSS-treated LNCaP cells were cultured in 12-well plates and transiently transfected with 1 μ g of the ROMO1-green fluorescent protein (GFP) reporter containing wild-type (WT) or mutant (M) E boxes. ADT-treated LNCaP and C4-2 cells were treated with DMSO, 30 μ M JQ1, or 30 μ M OTX-15 for 24 h. The promoter function was analyzed using FACS (BD Biosciences), and relative GFP MFI values were measured by FACS using FACSDiva software (BD Biosciences) and normalized to the value of the vehicle. Three independent experiments were performed in triplicate.

2.17. Enzyme-linked immunosorbent assay (ELISA)

Serum ROMO1 titration was performed using the human ROMO1 ELISA kit (MBS4502277; MyBioSource) according to the manufacturer's instructions. Sera from healthy donors (27 samples), patients with primary PCa (22 samples), and metastatic PCa patients (19 samples) were collected from Taipei Medical University-Wan Fang Hospital (Taipei, Taiwan). Written informed consent was obtained from all patients, and the study was approved by the Taipei Medical University Joint Institutional Review Board (approval no. N202201057) in accordance with the *Declaration of Helsinki*. Clinical stage information for patients selected for circulating ROMO1 measurements is shown in Supplemental file 4.

2.18. Statistical analysis

All data are presented as the mean \pm standard error of the mean (SEM). Statistical calculations were performed with GraphPad Prism analytical tools (GraphPad Software). Differences between individual groups were determined using Student's *t*-test or a one-way analysis of variance (ANOVA), followed by Bonferroni's post-test for comparisons among three or more groups. *p* values of <0.05 were considered statistically significant. A log-rank test was used for the survival curve analysis of the Taylor [36] PCa clinical datasets using GraphPad Prism, and hazard ratios of ROMO1 high ($n = 56$)/ROMO1 low ($n = 55$) were determined for each group. The method for determining cutoff values was predetermined by half the number of patients.

3. Results

3.1. Increased PKLR promotes altered mitochondrial function associated with malignant progression in PCa cells

PKLR has the potential to regulate mitochondrial function and promote oxidative stress in liver and kidney cancer [24,25]. Our earlier study showed that ADT induces upregulation of PKLR, which is associated with NED of PCa after ADT [26]. To determine the correlation of PKLR with the NEPC status, PKLR expression levels in a panel of PCa cell lines were validated. Results showed that increased PKLR was associated with NE markers and was enriched in MDV3100-resistant C4-2-MDVR, AR-negative PC3, and NEPC-like LASCPC01 cells compared to AR-positive LNCaP and C4-2 cells (Fig. 1A and Supplementary Fig. S1A). The specificity of PKLR-KD was shown in PC3 cells as inhibition of PKLR was associated with reduced NE markers and increased autophagy/mitophagy and apoptosis markers but no change in AR levels (Fig. 1B and Supplementary Fig. S1B). To determine the role of PKLR in mediating mitochondrial function in PCa cells, we validated mtDNA contents of PC3 cells with PKLR-KD and found that a reduced mtDNA content was associated with reduced ATP levels compared to control cells (Fig. 2C and D). Next, we analyzed the OCR of PC3 cells with PKLR-KD using a Seahorse XF24 analyzer to determine the role of PKLR in mitochondrial respiration. Results showed that OCR values were significantly downregulated in PKLR-KD cells compared to control cells (Fig. 1E). Consequently, we examined the effect of PKLR-KD on the proliferation of PC3 cells and found that cells with PKLR-KD had decreased cell proliferation (Supplementary Fig. S1C) and numbers of 3D spheres (Fig. 1F). We also found that PKLR-KD cells had reduced cell migration and invasion through Matrigel (Fig. 1G). Moreover, PKLR-KD cells showed reduced ROS production and cell cycle arrest in G₁ phase by FACS analysis (Fig. 1H and Supplementary Fig. S1D). In contrast, PKLR-overexpressing PC3 cells showed increased PKLR protein levels associated with upregulated NE markers and downregulated mitophagy/autophagy and apoptosis markers, but no change in AR levels (Supplementary Figs. S1E–F). Notably, overexpression of PKLR in PC3 cells resulted in partial increases in mtDNA contents, cellular ATP levels, OCR values, ROS production, cell proliferation, sphere formation, cell migration/invasion, and showed increased number of cells in S phase (Supplementary Fig. S1G–N), supporting an oncogenic role for PKLR-driven altered mitochondrial function in AR-negative PCa cells. We further stimulated PKLR levels in androgen-dependent LNCaP cells harboring a tetracycline-inducible PKLR vector (LNCaP/Tet-PKLR). We found that cells overexpressing PKLR may have higher mtDNA contents and ATP levels relative to a dose-dependent Dox response after Dox treatment (Fig. 1I–K). Moreover, PKLR overexpression also induced higher OCR values, cell proliferation, sphere formation, and cell migration/invasion in Dox-treated LNCaP/Tet-PKLR cells compared to control cells (Fig. 1L–O). To test the function of PKLR under ADT conditions, MDV3100-resistant C4-2-MDVR cells were used, and we found that increased PKLR levels in C4-2-MDVR cells were associated with upregulated NE markers, but no change in AR levels (Supplementary Fig. S2A). We also found that increased PKLR associated with upregulated mtDNA contents, cellular ATP levels, cell proliferation, sphere formation, cell migration/invasion, and ROS production compared to parental C4-2 cells; however, PKLR-KD eliminated these effects (Supplementary Figs. S2B–H). These data suggest that upregulation of PKLR may promote altered mitochondrial function, leading to malignant progression of PCa cells.

3.2. PKLR increases NED and alters mitochondrial function associated with ROMO1 upregulation

We aimed to understand the molecular mechanisms by which PKLR regulates mitochondrial function in PCa cells. Total mRNA was prepared from androgen-dependent LNCaP cells stably expressing the EV or PKLR

complementary (c)DNA, and an RNA-Seq analysis was performed to determine signaling pathways upregulated after PKLR overexpression (Supplementary file 2). RNA-Seq data were analyzed in a set of gene signatures collected from gene ontology (GO) classifications by gene set enrichment analysis (GSEA) and displayed as a ridge plot grouped using frequencies of fold change values for each gene set in PKLR-overexpressing cells compared to cells expressing the EV. We found that PKLR-overexpressing cells were significantly associated with an upregulated mitochondrial inner membrane protein-responsive gene signature (Supplementary Fig. S3A), supporting the role of PKLR in regulating mitochondrial function [25]. GSEA results were validated using The Cancer Genome Atlas (TCGA) PCa dataset and showed a robust correlation between PKLR upregulation and an increased mitochondrial inner membrane protein-responsive gene signature in PCa patients (Supplementary Fig. S3B). According to the GSEA results, we found that *ROMO1*, a ROS modulator, was the most important candidate gene that harbored the highest ranking metric score with a significant false discovery rate (FDR) and *p* value among the upregulated mitochondrial membrane protein components (Supplementary Fig. S3C). Volcano plots of RNA-Seq data from LNCaP cells transfected with PKLR cDNA or the EV confirmed that *ROMO1* mRNA was significantly upregulated in PKLR-overexpressing cells ($p = 0.0125$, Supplementary Fig. S3D), suggesting that upregulation of *ROMO1* is related to PKLR abundance in PCa cells.

To understand the association of *ROMO1* with PKLR, mRNA levels of *ROMO1* and PKLR were validated in a panel of PCa cell lines. Notably, MDV3100-resistant C4-2-MDVR, AR-negative PC3, and NEPC-like LASCPC01 cells expressed higher levels of *ROMO1* and PKLR than AR-positive VCaP, LNCaP, and C4-2 cells (Fig. 2A). Next, we investigated the functional role of PKLR in regulating *ROMO1* expression involved in PCa NED progression and mitochondrial function using LNCaP/Tet-PKLR cells with *ROMO1*-KD. We found that a dose-dependent increase in *ROMO1* mRNA was associated with PKLR overexpression in Dox-treated LNCaP/Tet-PKLR cells (Supplementary Fig. S3E). We also found that increased PKLR was associated with elevated *ROMO1*, and NE markers and decreased mitophagy/autophagy and apoptotic protein markers, but no change in AR protein abundance (Fig. 2B and Supplementary Fig. S3F). Moreover, *ROMO1*-KD expressed in PKLR-overexpressing cells exhibited decreased *ROMO1* associated with decreased NE markers and increased mitophagy/autophagy and apoptotic protein markers, but no change in AR protein levels (Fig. 2C and Supplementary Fig. S3G). We also found that mtDNA contents, cellular ATP levels, and the MMP were downregulated in PKLR-overexpressing cells with *ROMO1*-KD (Fig. 2D–F). Importantly, the OCR was significantly upregulated following PKLR overexpression, whereas it was downregulated in *ROMO1*-KD cells (Fig. 2G). These data suggest that PKLR induces mitochondrial function in PCa possibly through *ROMO1* activation. We further examined whether PKLR mediates PCa tumorigenesis through *ROMO1* upregulation *in vivo*. Male nude mice were subcutaneously injected with LNCaP/Tet-PKLR cells stably transfected with *ROMO1* or control shRNA, and mice were treated with Dox in drinking water. We observed stimulated tumor growth in mice injected with LNCaP/Tet-PKLR cells harboring control shRNA in the presence of Dox; however, mice injected with LNCaP/Tet-PKLR cells harboring *ROMO1* shRNA and treated with Dox showed significantly attenuated tumor growth (Fig. 2H) and tumor weights (Fig. 2I), compared to mice injected with control shRNA and treated with Dox. Interestingly, the PKLR protein abundance in cells was associated with upregulated *ROMO1*, NE (*ENO2*), and proliferation (*KI67*) markers and a decrease in AR-responsive protein (*NKX3-1*) and apoptotic protein (cleaved caspase-3) in Dox-treated mice, whereas *ROMO1*-KD reduced the abundance of *ROMO1*, *ENO2*, and *KI67* but increased *NKX3-1* and cleaved caspase-3 in Dox-treated mice, as confirmed by IHC staining (Fig. 2J and K). These results suggest that PKLR overexpression may upregulate mitochondrial function and NE marker expression; however, *ROMO1*-KD decreased mitochondrial function and NE marker

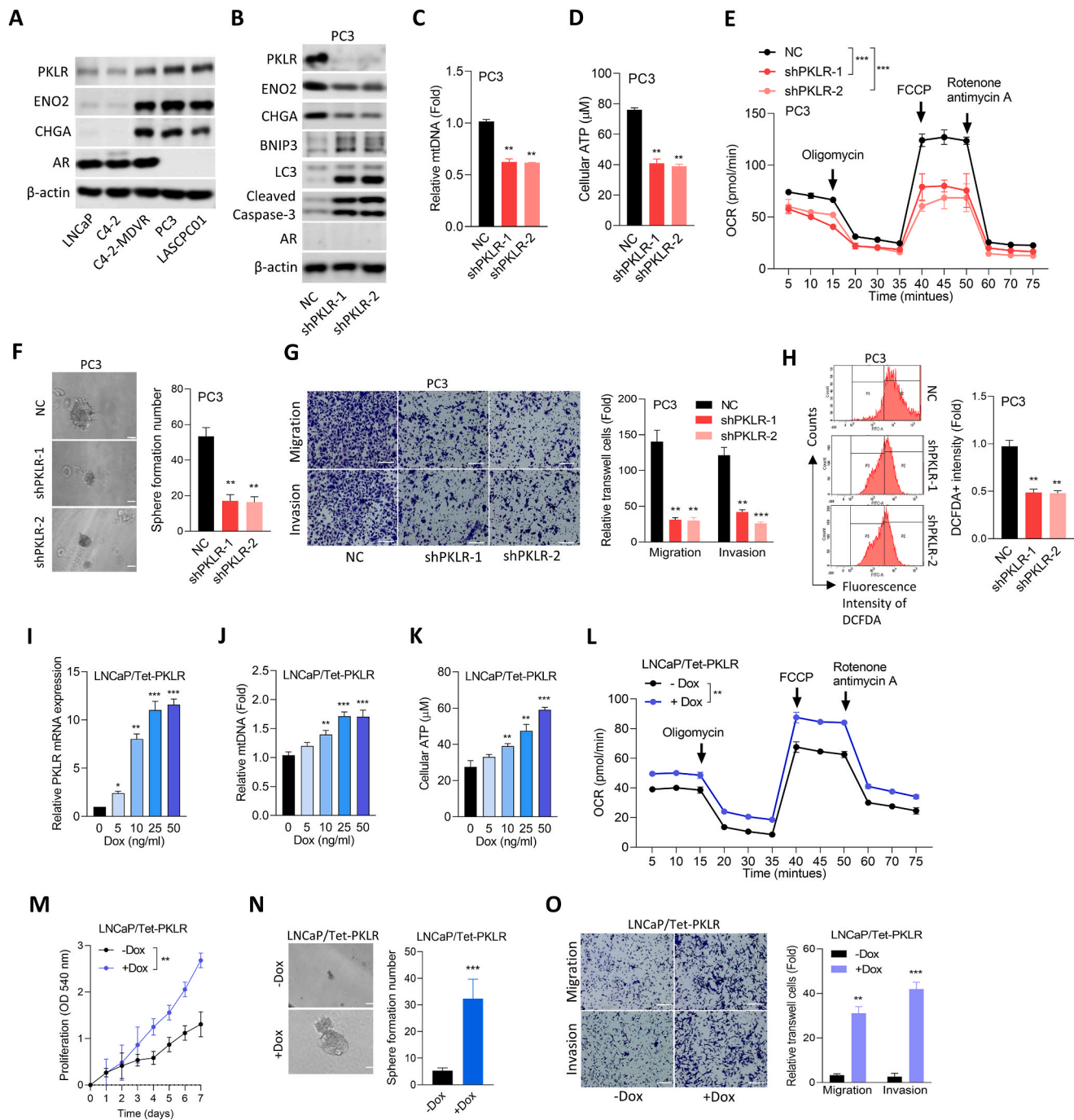


Fig. 1. PKLR upregulates mitochondrial function and increases aggressiveness of prostate cancer (PCa) cells.

(A) Representative immunoblots of PKLR, ENO2, CHGA, and AR protein levels in various PCa cells. (B) Representative immunoblots of PKLR, ENO2, CHGA, BNIP3, LC3, cleaved caspase-3, and AR protein levels in PC3 cells stably expressing the non-targeting control (NC) or PKLR shRNA vector. (C and D) Relative mtDNA contents (C) and cellular ATP levels (D) in PC3 cells stably expressing the NC or PKLR shRNA vector. * vs. the NC. (E) Oxygen consumption rate (OCR) measurements in PC3 cells stably expressing the NC or PKLR shRNA vector using a Seahorse XF24 extracellular flux analyzer following the sequential addition of inhibitors of mitochondrial function: oligomycin, FCCP, and a combination of rotenone and antimycin A. $n = 3$ per group. * vs. the NC. (F and G) Three-dimensional sphere-formation (F) and migration and invasion through Matrigel (G) assays of PC3 cells stably expressing the NC or PKLR shRNA vector. $n = 5$ per group. * vs. the NC. Scale bars represent 20 μ m (F) and 100 μ m (G), respectively. (H) Reactive oxygen species (ROS) analysis in PC3 cells stably expressing the NC or PKLR shRNA vector, stained with DCFDA, and then analyzed for changes in their fluorescent profile using flow cytometry. $n = 3$ per group. (I–K) Relative PKLR mRNA (I) and mtDNA contents (J), and cellular ATP levels (K) in LNCaP/Tet-PKLR cells with different doses of doxycycline (Dox) treatment for 24 h * vs. -0 ng/ml Dox. (L) OCR measurements in LNCaP/Tet-PKLR cells with 25 ng/ml of Dox treatment for 24 h following sequential addition of inhibitors of mitochondrial function. $n = 3$ per group. * vs. -Dox. (M and N) Cell proliferation (M) and three-dimensional sphere-formation (N) assays in LNCaP/Tet-PKLR cells with 25 ng/ml of Dox treatment for 6 days. $n = 8$ per group. * vs. -Dox. Scale bars represent 20 μ m. (O) Migration and invasion through Matrigel assays in LNCaP/Tet-PKLR cells with 25 ng/ml of Dox treatment for 12 h $n = 5$ per group. * vs. -Dox. Scale bars represent 100 μ m. Data from relative mtDNA contents, cellular ATP levels, proliferation, migration, invasion through Matrigel assays, DCFDA intensity, and OCR measurements are presented as the mean \pm SEM of three independent experiments. * $p < 0.05$, ** $p < 0.01$, and *** $p < 0.001$, by a one-way ANOVA.

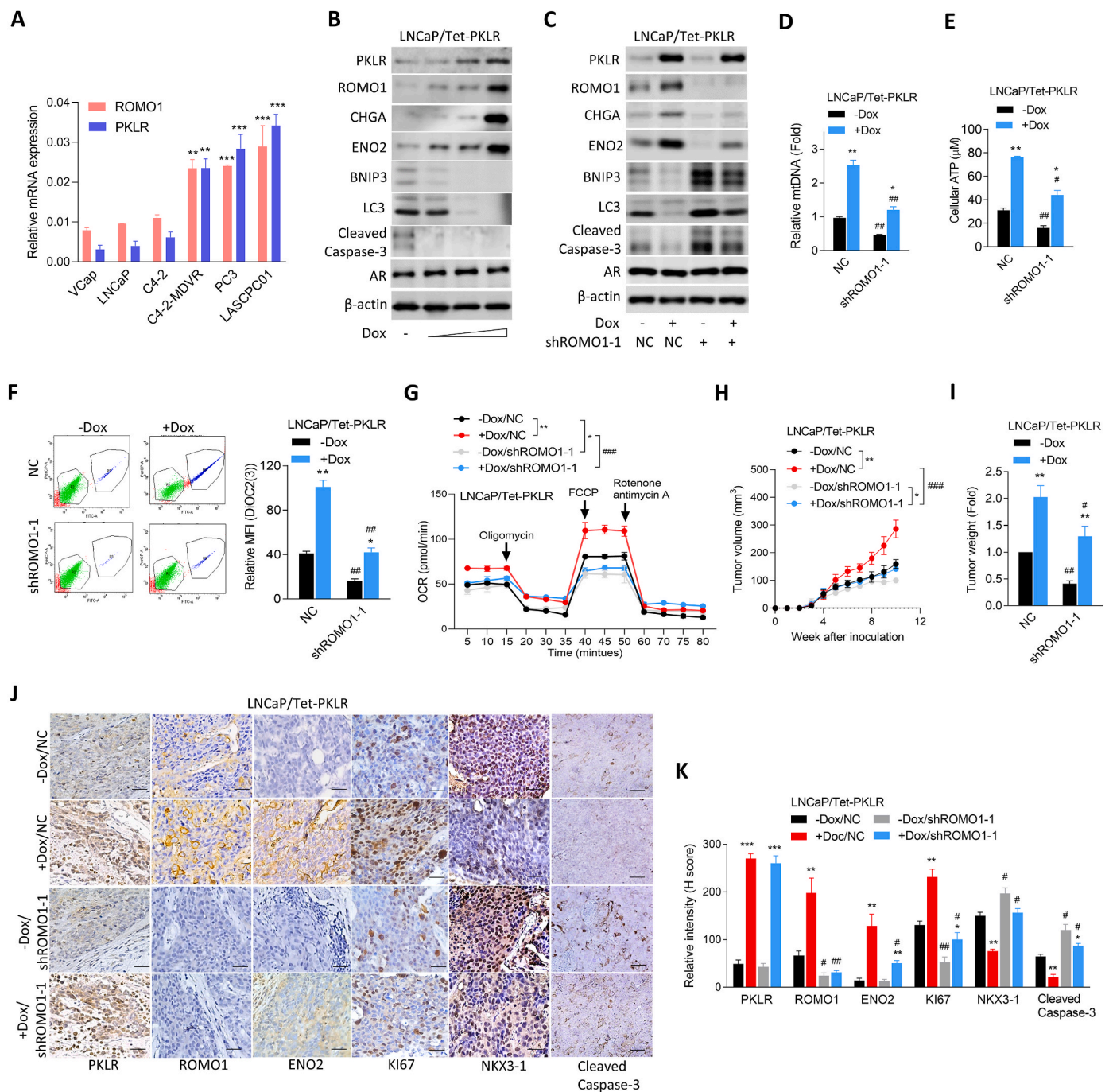


Fig. 2. PKLR/ROMO1 mediates mitochondrial function and the neuroendocrine (NE) differentiation potential of prostate cancer (PCa) cells. (A) Relative mRNA levels of ROMO1 and PKLR in various PCa cells by an RT-qPCR. * vs. VCaP, by a one-way ANOVA. (B) Protein levels of PKLR, ROMO1, CHGA, ENO2, BNIP3, LC3, cleaved caspase-3, and AR in LNCaP/Tet-PKLR cells with 0, 5, 10, and 25 ng/ml of doxycycline (Dox) treatment for 24 h by WB. (C) Protein abundance of PKLR, ROMO1, CHGA, ENO2, BNIP3, LC3, cleaved caspase-3, and AR in LNCaP/Tet-PKLR cells stably expressing the non-targeting control (NC) or ROMO1 shRNA vector following 25 ng/ml of Dox treatment for 24 h by WB. (D and E) Relative mtDNA contents (D) and cellular ATP levels (E) in LNCaP/Tet-PKLR cells stably expressing the NC or ROMO1 shRNA vector following 25 ng/ml of Dox treatment for 24 h * vs. -Dox; # vs. the NC, by a two-way ANOVA. (F) Relative mitochondrial membrane potential (MMP) in LNCaP/Tet-PKLR cells stably expressing the NC or ROMO1 shRNA vector following 25 ng/ml of Dox treatment for 24 h. Cells were stained with DiOC₂(3)-FTIC, and then analyzed for changes in their fluorescent profile by flow cytometry. Results of the quantitative analysis of DiOC₂(3)-FTIC staining are shown as the relative median fluorescence intensity (MFI). * vs. -Dox; # vs. the NC, by a two-way ANOVA. (G) Oxygen consumption rate (OCR) measurements of LNCaP/Tet-PKLR cells stably expressing the NC or ROMO1 shRNA vector following 25 ng/ml of Dox treatment for 24 h and sequential addition of inhibitors of mitochondrial function. *n* = 3 per group. * vs. -Dox; # vs. the NC, by a two-way ANOVA. (H and I) Tumor growth analysis of mice subcutaneously inoculated with LNCaP/Tet-PKLR cells. Dox-treated mice received Dox at a concentration of 2 mg/ml in drinking water for 10 weeks. Tumor sizes were monitored once a week (H) and tumor weights (I) were obtained at the end of the experiment (*n* = 5 mice per group). * vs. -Dox; # vs. the NC, by a two-way ANOVA. (J and K) IHC staining (J) and relative intensities (K) of PKLR, ROMO1, ENO2, KI67, NKX3-1, and cleaved caspase-3 in subcutaneous tumors from (H). * vs. -Dox; # vs. the NC, by a two-way ANOVA. Scale bars (J) represent 100 μ m. Data from relative mRNA expression, mtDNA contents, cellular ATP levels, MFIs of FTIC, and OCR measurements are presented as the mean \pm SEM of three independent experiments. **p* < 0.05, ***p* < 0.01, and ****p* < 0.001.

expression in PKLR-overexpressing cells. Taken together, our findings suggest that PKLR may be an upstream regulator of ROMO1, and ROMO1 is required for mitochondrial function and malignant progression in PCa.

3.3. ROMO1-upregulated NED is associated with altered mitochondrial function in PCa

Although ROMO1 was shown to be involved in regulating ROS production [32] and to be associated with the malignant progression of lung, bladder, and colorectal cancers [37–39], the functional role of ROMO1 in NED of PCa remains unknown. To determine the role of ROMO1 in affecting NED in AR-positive cells, ROMO1 cDNA was overexpressed in LNCaP cells. We found that ROMO1 overexpression in LNCaP cells increased NE markers associated with stem cell markers (Fig. 3A and B and Supplementary Fig. S3H), supporting NED in PCa being correlated with abundance of stem cell markers [40]. We also found that ROMO1 cDNA overexpression in LNCaP cells upregulated cell proliferation and 3D sphere formation (Fig. 3C and D), supporting the highly proliferative nature of NEPC cells [41]. To determine whether upregulation of ROMO1 mediates mitochondrial function, we examined the MMP in ROMO1-overexpressing LNCaP cells by staining with a mitochondrial stress indicator (DiOC₂(3)) and flow cytometric measurements. Results showed that the MMP was upregulated upon ROMO1 overexpression, as indicated by DiOC₂(3) accumulation (Fig. 3E). Moreover, higher mtDNA contents and ATP levels were found in ROMO1-overexpressing cells (Fig. 3F and G). In contrast, AR-negative PC3 cells with ROMO1-KD were found to have reduced NE and stem cell markers (Fig. 3H and I and Supplementary Fig. S3I). Reduced cell proliferation and 3D sphere formation as well as decreased mtDNA and cellular ATP contents were detected in PC3 cells with ROMO1-KD (Fig. 3J–M). A reduction in the MMP was observed in PC3 cells harboring ROMO1-KD (Fig. 3N). Importantly, ROMO1 overexpression in LNCaP cells resulted in upregulation of OCR values, whereas ROMO1-KD PC3 cells showed reduced OCR values, as determined with the Seahorse XF24 analyzer (Fig. 3O–P). These data suggest that ROMO1 overexpression may upregulate NED progression and change mitochondrial function in PCa.

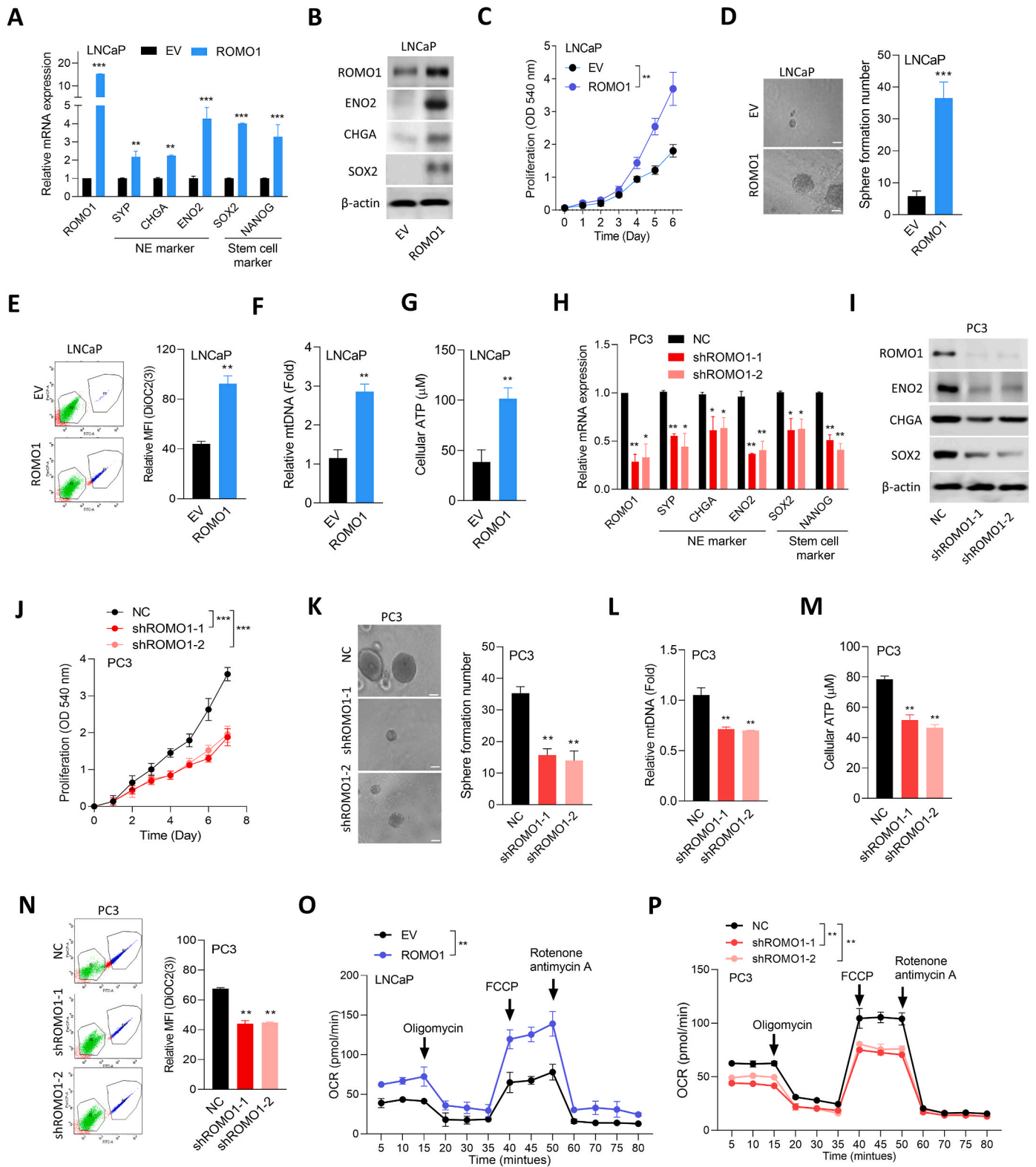
3.4. ADT induces ROMO1 expression, and its abundance correlates with NE phenotype and lineage plasticity in PCa

To study the clinical relevance of PKLR/ROMO1 in PCa, we analyzed abundance of PKLR and ROMO1 by IHC staining in a PCa TMA, including 40 cases of primary PCa and nine cases of benign prostatic tissues (CA4; SuperBioChips Laboratories). The IHC analysis showed a positive correlation between ROMO1 abundance and PKLR in tumor cells according to Spearman's rank correlation coefficient ($R = 0.3498$; $p = 0.0269$, Fig. 4A and B). We also found that PCa samples with higher tumor grades exhibited significantly higher abundance of PKLR and ROMO1, according to a Chi-squared test (Fig. 4C and D). The mean expression correction was validated using the Taylor and TCGA PCa datasets, which showed that PKLR abundance were positively correlated with ROMO1 (Supplementary Figs. S4A–B). In the GSE21036 PCa dataset, ROMO1 mRNA abundance were significantly higher in primary tumor samples than in normal prostate tissues and further increased in metastatic tumors (Fig. 4E). The Kaplan-Meier analysis showed that PCa patients whose tumors had higher ROMO1 mRNA abundance survived for shorter periods than those with low ROMO1 mRNA abundance, according to a log-rank test of the GSE21036 PCa dataset (hazard ratio ROMO1 high/ROMO1 low = 2.843; Fig. 4F). In addition, the upregulated mean ROMO1 abundance was associated with higher cancer stages and Gleason scores in the GSE21036 PCa dataset (Supplementary Figs. S4C–D). We next examined ROMO1 mRNA abundance in an RNA-Seq dataset (GSE48403) of paired PCa samples before and after ADT, and found that ROMO1 was significantly elevated in patients after ADT

(Fig. 4G). In line with AR inhibition, charcoal-stripped serum (CSS-containing medium) is widely used to create a hormone-free cell culture medium to mimic ADT treatment in PCa patients [42]. AR-positive LNCaP cells treated with CSS-containing medium showed abundant PKLR mRNA, which correlated with the upregulated mRNA abundance of ROMO1, NE (SYP, CHGA, and ENO2), and stem cell (SOX2 and NANOG) markers, but with no change in AR levels (Fig. 4H). Conversely, decreased mRNAs of PKLR, ROMO1, NE, and stem cell markers but no change in AR were observed in CSS-treated cells treated with AR ligand, DHT (Fig. 4H). For long-term AR antagonist treatment of cells, MDV3100, which specifically inhibits AR signaling, was used to treat C4-2 cells [43,44]. Consistently, C4-2-MDVR cells showed abundant ROMO1 mRNA, which was associated with upregulated mRNA abundance of PKLR, NE, and stem cell markers but with no change in AR (Fig. 4I). An abundance of the PKLR protein was observed in CSS-treated LNCaP and C4-2-MDVR cells and was correlated with abundant ROMO1 and NE markers, whereas ROMO1-KD reduced the abundance of ROMO1 and NE marker proteins but with no change in AR (Fig. 4J and K and Supplementary Figs. S4E–F). The GSEA of TCGA PCa database validated that upregulation of NEPC-responsive gene signatures was positively correlated with PCa tissues expressing higher PKLR and ROMO1 mRNAs (Fig. 4L). Significantly, ROMO1 mRNA abundance was higher in NEPC patients than in PCa adenocarcinoma patients in the NEPC dataset [45] by a z-score analysis (Fig. 4M). Moreover, highly abundant ROMO1 PCa samples were positively associated with gene signatures involved in neuronal developmental responsiveness (KEGG, GO, and REACTOME) and negatively correlated with androgen responsiveness (Nelson [6], Wang [46], Doane [47], PID, and GO) based on verification of the GSEA in TCGA PCa dataset (Fig. 4N), supporting the hypothesis that ROMO1 upregulation was correlated with NEPC progression. We further investigated how PKLR/MOMO1 signaling promotes malignant progression in AR-negative and ADT-resistant cells. PKLR shRNA was expressed in PC3 and C4-2-MDVR cells and further rescued with ROMO1 cDNA. Results showed that cells with PKLR-KD had reduced ROMO1, and NE marker proteins and increased autophagy/mitophagy and apoptosis markers, whereas rescue by ROMO1 reversed these effects, but AR protein was unchanged (Supplementary Figs. S5A–B). We also found that PKLR-KD suppressed cell migration, invasion, and proliferation, whereas ROMO1 overexpression in PKLR-KD cells exhibited increases in these malignant features (Supplementary Figs. S5C–F). Based on these findings, ROMO1 may be upregulated in PCa after ADT and contribute to PKLR-driven NED and malignant progression.

3.5. ADT induces nuclear function of PKLR and drives PKLR/MYCN/MAX interactions

To explore the clinical significance between PKLR and ROMO1 in PCa after ADT, ADT-induced PKLR/ROMO1 signaling was confirmed through an analysis of consecutive tissue sections of prostate tumor samples isolated from patients before and after ADT. We found that the abundance of nuclear PKLR and cytoplasmic ROMO1 were higher in prostate tumors from patients who had received ADT than in those from hormone-naïve patients according to IHC staining (Fig. 5A and B). These results suggest that PKLR protein in PCa may be translocated into the nucleus after ADT and may be associated with ROMO1 upregulation. We next validated nuclear PKLR abundance by treating AR-positive LNCaP cells with CSS-containing medium to induce ADT. IF staining results showed that the intensity of the nuclear PKLR protein was positively correlated with nuclear DAPI (Supplementary Figs. S6A–B), confirming the accumulation of nuclear PKLR in cells after ADT. To understand relevant pathways after PKLR activation, we analyzed RNA-Seq data in LNCaP cells expressing EV or PKLR cDNA by GSEA for gene signatures in response to potential signaling pathways. Based on the GSEA, the enrichment distribution was shown as a grouped ridge graph, indicating that the upregulated MYC-targeted responsive gene signature was the



(caption on next page)

Fig. 3. Activated ROMO1 mediates neuroendocrine (NE) differentiation and mitochondrial function of prostate cancer (PCa) cells.

(A) Relative mRNA levels of ROMO1, NE (SYP, CHGA, and ENO2) markers, and stem cell (SOX2 and NANOG) markers in LNCaP cells stably expressing an empty vector (EV) or ROMO1 cDNA vector by an RT-qPCR. * vs. the EV. (B) Relative protein levels of ROMO1, ENO2, CHGA, and SOX2 in LNCaP cells stably expressing the EV or ROMO1 cDNA vector by WB. (C and D) Cell proliferation (C) and three-dimensional sphere-formation (D) assays of LNCaP cells stably expressing the EV or ROMO1 cDNA vector for 6 days. $n = 8$ per group. * vs. the EV. Scale bars (D) represent 20 μm . (E) Relative mitochondrial membrane potential (MMP) of LNCaP cells stably expressing the EV or ROMO1 cDNA vector. Cells were stained with DiOC₂(3)-FTIC, and then analyzed for changes in their fluorescent profile by flow cytometry. Results of the quantitative analysis of DiOC₂(3)-FTIC staining are shown as the relative median fluorescence intensity (MFI). * vs. the EV. (F and G) Relative mtDNA contents (F) and cellular ATP levels (G) in LNCaP cells stably expressing the EV or ROMO1 cDNA vector. * vs. the EV. (H) Relative mRNA levels of ROMO1, NE, and stem cell markers in PC3 cells stably expressing the non-targeting control (NC) or ROMO1 shRNA vector by an RT-qPCR. * vs. the NC. (I) Relative protein levels of ROMO1, ENO2, CHGA, and SOX2 in PC3 cells stably expressing the NC or ROMO1 shRNA vector by WB. (J and K) Cell proliferation (J) and three-dimensional sphere-formation (K) assays in PC3 cells stably expressing the NC or ROMO1 shRNA vector for 6 days. $n = 8$ per group. * vs. the NC. Scale bars (K) represent 20 μm . (L and M) Relative mtDNA contents (L) and cellular ATP levels (M) in PC3 cells stably expressing the NC or ROMO1 shRNA vector. * vs. the NC. (N) Relative MMP in PC3 cells stably expressing the NC or ROMO1 shRNA vector. * vs. the NC. (O and P) Oxygen consumption rate (OCR) measurements of LNCaP cells stably expressing the EV or ROMO1 cDNA vector (O) or PC3 cells stably expressing the NC or ROMO1 shRNA vector (P) following sequential addition of inhibitors of mitochondrial function. $n = 3$ per group. * vs. the EV (O) or the NC (P). Data from relative mRNA expression, proliferation, migration, invasion through Matrigel assays, mtDNA contents, cellular ATP levels, MFIs of FTIC, and OCR measurements are presented as the mean \pm SEM of three independent experiments. * $p < 0.05$, ** $p < 0.01$, and *** $p < 0.001$, by a one-way ANOVA.

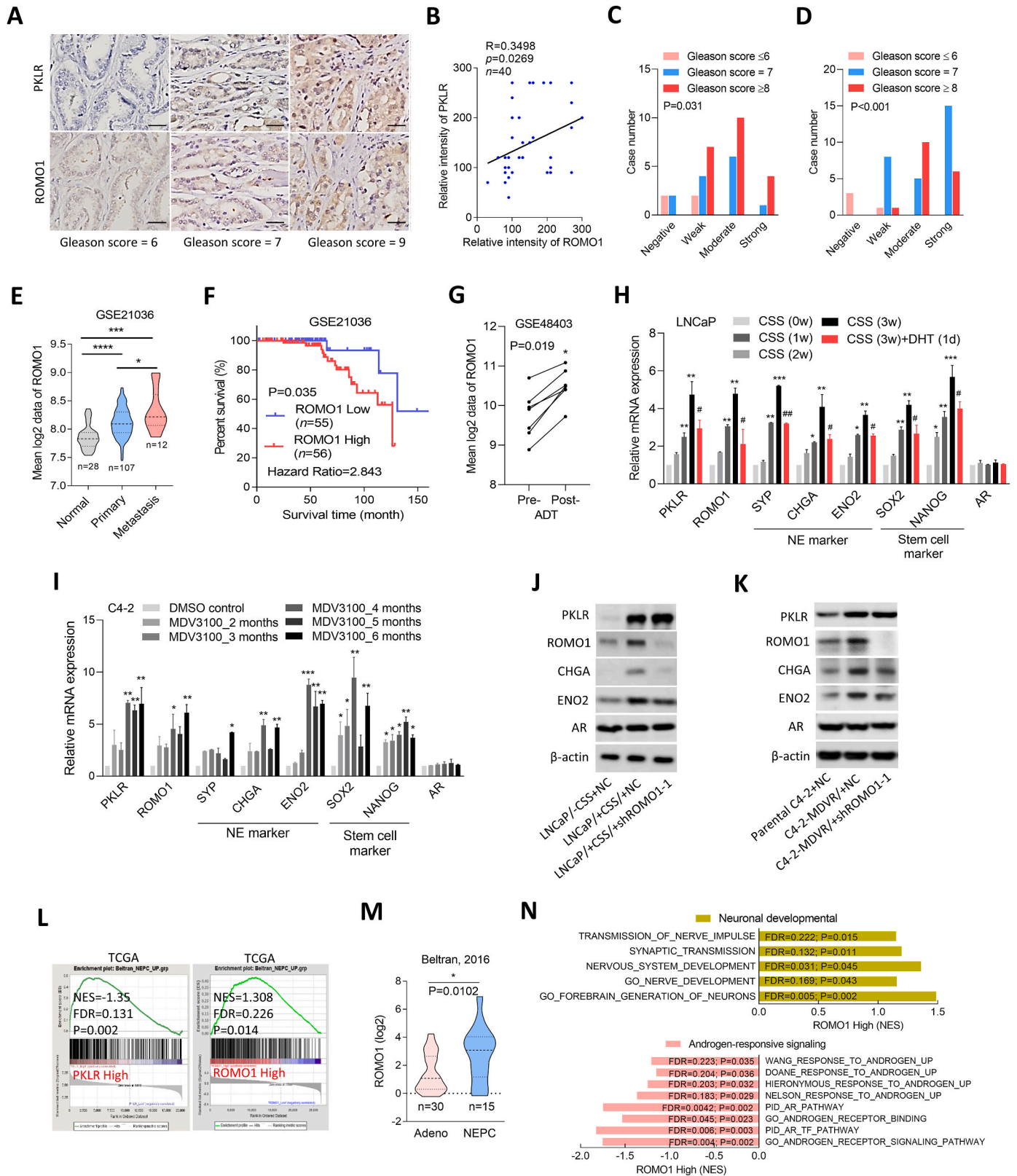
highest ranked and was significantly more positive in PKLR-expressing cells compared to EV-expressing cells (Supplementary Figs. S6C–D). Although MYC activation is the most common molecular change in human cancers [48], experimental evidence has shown that MYC and MYCN, a transcription factor in the same family, are functionally interchangeable [49], and MYCN is more specific for NED of PCa [41, 50]. Interestingly, we found that PKLR protein and mRNA levels were higher in C4-2-MDVR cells than in control parental C4-2 cells and were significantly correlated with abundance of ROMO1, MYCN, and MAX, but not MYC (Fig. 5C and D and Supplementary Fig. S6E). C4-2-MDVR cells treated with MYCN-specific siRNA showed reductions in PKLR, ROMO1, MYCN, and MAX proteins and mRNAs; however, MYC siRNA treatment reduced MYC and MAX, but not PKLR, ROMO1, or MYCN (Fig. 5C and D and Supplementary Fig. S6E). We also found that silencing of MYCN in NEPC-like LASCPC01 cells resulted in decreased abundance of PKLR, ROMO1, MYCN, and MAX proteins compared to MYC-KD cells (Fig. 5E and Supplementary Fig. S6F). These data suggest possible correlations among PKLR, ROMO1, MYCN, and MAX proteins in PCa cells after ADT resistance or NED progression. We further treated LASCPC01 cells with two putative MYCN inhibitors, JQ1 [33] and OTX-15 [34], a BET inhibitor, to examine relationships among PKLR, ROMO1, MYCN, and MAX proteins. We found that a dose-dependent reduction in PKLR protein was associated with decreased abundance of ROMO1, MYCN, and MAX in cells treated with increasing concentrations of JQ1 or OTX-15 (Fig. 5F and Supplementary Figs. S6G–H). Moreover, CSS-treated LNCaP cells showed abundant PKLR, ROMO1, MYCN, and MAX mRNA and protein levels, whereas CSS-treated cells treated with JQ1 or OTX-15 exhibited reduced abundance of PKLR, ROMO1, MYCN, and MAX (Supplementary Figs. S6I–J). Consistently, C4-2-MDVR cells treated with JQ1 or OTX-15 showed downregulation of PKLR, ROMO1, MYCN, and MAX mRNAs and proteins (Fig. 5G and H and Supplementary Fig. S6K). These results suggest that MYCN may contribute to PKLR-mediated ROMO1 abundance in PCa cells after ADT and that BET inhibitor treatment may suppress this effect.

To verify possible interactions of nuclear PKLR with MYCN and MAX proteins in NEPC-like PCa, LASCPC01 cells were subjected to IP-WB analyses, followed by NC, MYCN, or MYC siRNA treatment. Notably, stable interactions between nuclear PKLR/MYCN/MAX proteins in LASCPC01 cells were observed by IP of nuclear PKLR or MYCN proteins and immunoblotting of PKLR, MYCN, or MAX proteins; however, LASCPC01 cells transfected with MYCN siRNA but not MYC siRNA exhibited reduced nuclear PKLR/MYCN/MAX protein interactions (Fig. 5I and Supplementary Figs. S7A–B). Consistently, reduced interactions among these proteins were observed in LASCPC01 cells treated with JQ1 or OTX-15 (Fig. 5J and Supplementary Figs. S7C–D). We also found that C4-2-MDVR cells displayed enhanced interactions between nuclear PKLR/MYCN/MAX proteins compared to parental C4-2 cells, whereas JQ1 or OTX-15 treatment inhibited their interaction, as

analyzed by IP of nuclear PKLR or MYCN proteins and immunoblotting of PKLR, MYCN, or MAX proteins (Fig. 5K and Supplementary Figs. S7E–F). These data suggest that nuclear PKLR/MYCN/MAX complex interactions are upregulated in PCa after ADT resistance or NED progression.

3.6. ADT-activated PKLR/MYCN complex upregulates ROMO1, CHGA, SYP, and ENO2

We hypothesized that nuclear PKLR may be associated with the MYCN/MAX complex as a transcriptional cofactor that binds to ROMO1 regulatory sequence. We downloaded the ChIP-Seq data from the GEO (GSM1711858 and GSM2915909) and analyzed potential binding of MYCN and MAX to ROMO1 using the Genome Browser (Genomics Institute). Results showed that MYCN and MAX appeared to bind to multiple sites on ROMO1 (Supplementary Fig. S8A). Given that E-box is a putative binding site for the MYCN/MAX complex [51], we searched for sequences resembling E-box in the putative ROMO1 regulatory sequence region. Notably, we identified five candidate E-boxes upstream of the ROMO1 transcription start site and one downstream E-box (Fig. 6A). To determine whether nuclear PKLR/MYCN directly binds to ROMO1 in PCa after ADT resistance, ChIP assays were performed using nuclear extracts from C4-2-MDVR cells in the presence of JQ1 or OTX-15. We found that nuclear PKLR and MYCN significantly bound to ROMO1 at E-boxes 2, 3, and 6 by IP of nuclear PKLR or MYCN proteins using PKLR and MYCN antibodies in C4-2-MDVR cells (Fig. 6B and Supplementary Fig. S9A). We also found that the binding capacity of the same site was diminished after treatment of cells with JQ1 or OTX-15 (Fig. 6B and Supplementary Fig. S9A), consistent with reductions in ROMO1 protein and mRNA in C4-2-MDVR cells in response to JQ1 or OTX-15 (Fig. 5G and H). In addition, promoter reporter assays were performed using DNA constructs containing a single wild-type (WT) or mutant (M) E-box from ROMO1 cloned into a GFP reporter plasmid (Fig. 6A). Notably, C4-2-MDVR and LASCPC01 cells treated with JQ1 or OTX-15 showed repressed reporter activity of WT E-boxes 2, 3, and 6, and greater repression was observed in cells harboring E-box mutants (Fig. 6C and Supplementary Fig. S9B). Moreover, enhancement of reporter activity was found in LNCaP cells treated with CSS; however, CSS-treated LNCaP cells treated with JQ1 or OTX-15 showed suppressed reporter activity of the WT E-box 2, 3, and 6 reporters relative to untreated cells (Supplementary Fig. S9C). We also found downregulated reporter activities in these E-box mutants compared to the WTs, regardless of CSS treatment, and greater suppression of reporter activity was found in these E-box mutants in the presence of JQ1 or OTX-15 (Supplementary Fig. S9C). In summary, these data suggest a mechanism by which the nuclear PKLR/MYCN complex may directly interact with ROMO1 promoter by binding to E-boxes 2, 3, and 6, to enhance ROMO1 transcription in PCa after ADT or NED progression.



(caption on next page)

Fig. 4. Androgen-deprivation therapy (ADT) upregulates PKLR/ROMO1 involved in neuroendocrine (NE) differentiation of prostate cancer (PCa). (A) IHC staining with antibodies specific for PKLR and ROMO1 in a PCa TMA (CA4, $n = 40$) with different Gleason scores. Scale bars represent 100 μm . (B) Correlation analysis of the intensities of PKLR and ROMO1 of a PCa TMA from (A). R , correlation coefficient; p , two-tailed p value. Significance was determined by correlation XY analyses using GraphPad Prism. (C and D) Analysis of PKLR and ROMO1 expression associated with different grades in clinical PCa samples from (A). The intensity of PKLR (C) and ROMO1 (D) staining was semiquantitatively scored as negative, weakly positive, moderately positive, and strongly positive. p values were calculated by a Chi-squared test. (E) Mean levels of ROMO1 mRNA of normal ($n = 28$), primary ($n = 98$), and metastatic ($n = 13$) human prostate samples from the GSE21036 PCa dataset. * vs. normal tissues. * $p < 0.05$, *** $p < 0.001$, and **** $p < 0.0001$ by Student's t -test. (F) Kaplan-Meier analyses of ROMO1 alterations in the GSE21036 PCa dataset. Significance was determined by a log-rank (Mantel-Cox) test. (G) Mean expression of ROMO1 in paired PCa samples pre- and post-ADT from the GSE48403 PCa dataset. * vs. pre-ADT. * $p < 0.05$ by Student's t -test. (H) Relative mRNA levels of PKLR, ROMO1, NE, stem cell markers, and AR in LNCaP cells after treatment with CSS-containing medium for 1–3 weeks followed by treatment with 10 nM DHT in week 3 for 1 day. * vs. CSS (0 weeks); # vs. CSS (3 weeks). (I) Relative mRNA levels of PKLR, ROMO1, NE, stem cell markers, and AR in C4-2 cells after treatment with MDV3100 for 2–6 months. * vs. the DMSO control. Data from relative mRNA levels are the mean \pm SEM of three independent experiments. * $p < 0.05$, ** $p < 0.01$ and *** $p < 0.001$ by a two-way ANOVA. (J and K) Protein levels of PKLR, ROMO1, CHGA, ENO2, and AR in LNCaP cells stably expressing the non-targeting control (NC) or ROMO1 shRNA vector after treatment with CSS-containing medium for 1 week (J) or C4-2-MDVR cells stably expressing the NC or ROMO1 shRNA vector (K) by WB. (L) GSEA of TCGA PCa dataset revealed significant correlations between higher PKLR and ROMO1 expression in PCa tissues with a gene signature responsive to NEPC. NES, normalized enrichment score; FDR, false discovery rate. (M) Comparison of mean expression of ROMO1 mRNA between patients with an adenocarcinoma and patients with NEPC in the Beltran PCa database. * $p < 0.05$ by Student's t -test. (N) GSEA of TCGA PCa dataset showing that higher ROMO1 expression in PCa tissues was positively correlated with neuronal development (top) and negatively correlated with androgen-responsive (bottom) gene signatures.

To explore the relationship of upregulation of the nuclear PKLR/MYCN/MAX complex in PCa cells after ADT, which involves enhancement of NED, we examined the abundance of NE markers in C4-2-MDVR and CSS-treated LNCaP cells following JQ1 or OTX-15 treatment. Significantly, we found that the abundance of NE marker (CHGA, SYP, and ENO2) mRNAs and proteins was upregulated in cells after ADT compared to untreated cells; however, ADT-treated cells treated with JQ1 or OTX-15 exhibited reduced NE marker abundance (Fig. 6D and Supplementary Figs. S10A–B). Consistently, we also observed reduced abundance of CHGA, SYP, and ENO2 mRNAs and proteins in LASCPC01 cells treated with JQ1 or OTX-15 (Supplementary Figs. S10C–D). These data suggest that targeting the PKLR/MYCN/MAX complex may suppress ADT-driven NED progression in PCa. Next, we searched the regulatory regions of CHGA, SYP, and ENO2 for sequences resembling putative E-boxes and identified multiple candidate E-boxes in the regulatory sequences of these genes by a ChIP-Seq analysis using the same ChIP-Seq data (GSM1711858 and GSM2915909) downloaded from GEO (Supplementary Figs. S8B–D). We searched for sequences resembling the E-box in the putative CHGA, SYP, and ENO2 regulatory sequence regions, and respectively identified five, four, and three putative E-boxes in CHGA, SYP, and ENO2 regulatory sequences (Fig. 6E). To determine whether the PKLR/MYCN complex directly binds to CHGA, SYP, and ENO2 in ADT-resistant PCa cells, ChIP assays were performed by IP of nuclear PKLR or MYCN proteins using PKLR and MYCN antibodies from nuclear extracts of C4-2-MDVR cells treated with JQ1 or OTX-15. We found significant binding of nuclear PKLR or MYCN to the regulatory sequences of CHGA, SYP, and ENO2 at E-boxes 2, 3, and 5 of CHGA, E-boxes 2 and 3 of SYP, and E-boxes 2 and 3 of ENO2 (Fig. 6F–H and Supplementary Figs. S10E–G). However, nuclear PKLR- or MYCN-binding signals were reduced in putative E-boxes of CHGA, SYP, and ENO2 in cells after JQ1 or OTX-15 treatment (Fig. 6F–H and Supplementary Figs. S10E–G). Promoter reporter assays were performed using DNA constructs containing a single WT or M E-box of CHGA, SYP, and ENO2 regulatory sequences cloned into a GFP reporter plasmid (Fig. 6E). JQ1- or OTX-15-treated C4-2-MDVR cells showed significantly repressed reporter activities of the putative WT E-boxes of CHGA (E-boxes 2, 3, and 5), SYP (E-boxes 2 and 3), and ENO2 (E-boxes 2 and 3) relative to untreated cells, and greater repressed reporter activity was observed in E-box mutants in cells treated with JQ1 or OTX-15 (Fig. 6I–K). These data suggest that the nuclear PKLR/MYCN complex may promote expression of NE markers by directly binding to E-boxes of CHGA, SYP, and ENO2, leading to NED of PCa after ADT.

3.7. Pharmacological targeting of nuclear PKLR/MYCN may be a possible therapeutic strategy for ADT-resistant or NE-like PCa

BET inhibitors were shown to be possible MYCN inhibitors [33,34].

Our findings suggest that BET inhibitors, such as JQ1 or OTX-15, can effectively inhibit PKLR/MYCN-driven ROMO1 function and may prevent PCa cells undergoing NED. We further examined the effects of BET inhibitors which *in vivo* targeted PKLR/MYCN/ROMO1 signaling in NEPC-like LASCPC01 cells (Fig. 7A). Notably, mice bearing LASCPC01 cells exhibited inhibition of tumor growth and tumor weights when treated with JQ1 compared to control mice (Fig. 7B–D). IHC staining showed that downregulation of PKLR protein in cells was associated with reduced abundance of MYCN, ROMO1, ENO2, and Ki67 proteins in LASCPC01-injected mice treated with JQ1 compared to control mice (Fig. 7E and F). These results suggest that targeting the PKLR/MYCN complex might be a promising therapeutic strategy for inhibiting progression of NE-like PCa. A diagnosis of NEPC mainly depends on characteristic histomorphologic features such as small-cell carcinoma and large-cell NE carcinoma, and not on CHGA or SYP expression as detected by IHC alone [40]. However, combined abundance of CHGA in serum and PCa tissues were shown to be correlated with the tumor stage and resistance to ADT [52]. The serum ROMO1 protein abundance was shown to be a potential diagnostic marker for lung cancer [53]; however, whether serum ROMO1 can be used as a prognostic biomarker in metastatic PCa patients remains unknown. We collected serum samples of PCa patients from Taipei Medical University-Wan Fang Hospital to measure serum ROMO1 protein abundance using a human ROMO1 ELISA kit. Results showed that serum ROMO1 concentrations were higher in metastatic PCa samples than in primary PCa or normal samples (Fig. 7G). Next, we performed IHC staining of PKLR, ROMO1, and SYP protein abundance in selected cases of each tissue and found that PKLR abundance was correlated with ROMO1 and SYP stimulation in metastatic PCa patients compared to primary PCa or normal samples (Fig. 7H). These data suggest that the serum ROMO1 abundance may be associated with PCa metastasis and NED progression. Taken together, our results provide a mechanism for ADT-induced nuclear translocation of PKLR, which interacts with the MYCN/MAX complex and leads to upregulation of ROMO1 and NE markers to change mitochondrial function and NED in PCa (Fig. 7I). We addressed the potential therapeutic and prognostic value of current AR signaling strategies by targeting the nuclear PKLR/MYCN complex and demonstrated that the serum ROMO1 abundance may be associated with the development of advanced PCa.

4. Discussion

A diagnosis of CRPC is based on a consecutive increase in prostate-specific antigen (PSA) levels and tumor growth under androgen-deprivation conditions [5]. There are no approved biomarkers for diagnosing the AR^{low/-} CRPC or NEPC subtypes, exacerbating the difficulty of early detection. We found an increased abundance of ROMO1 in

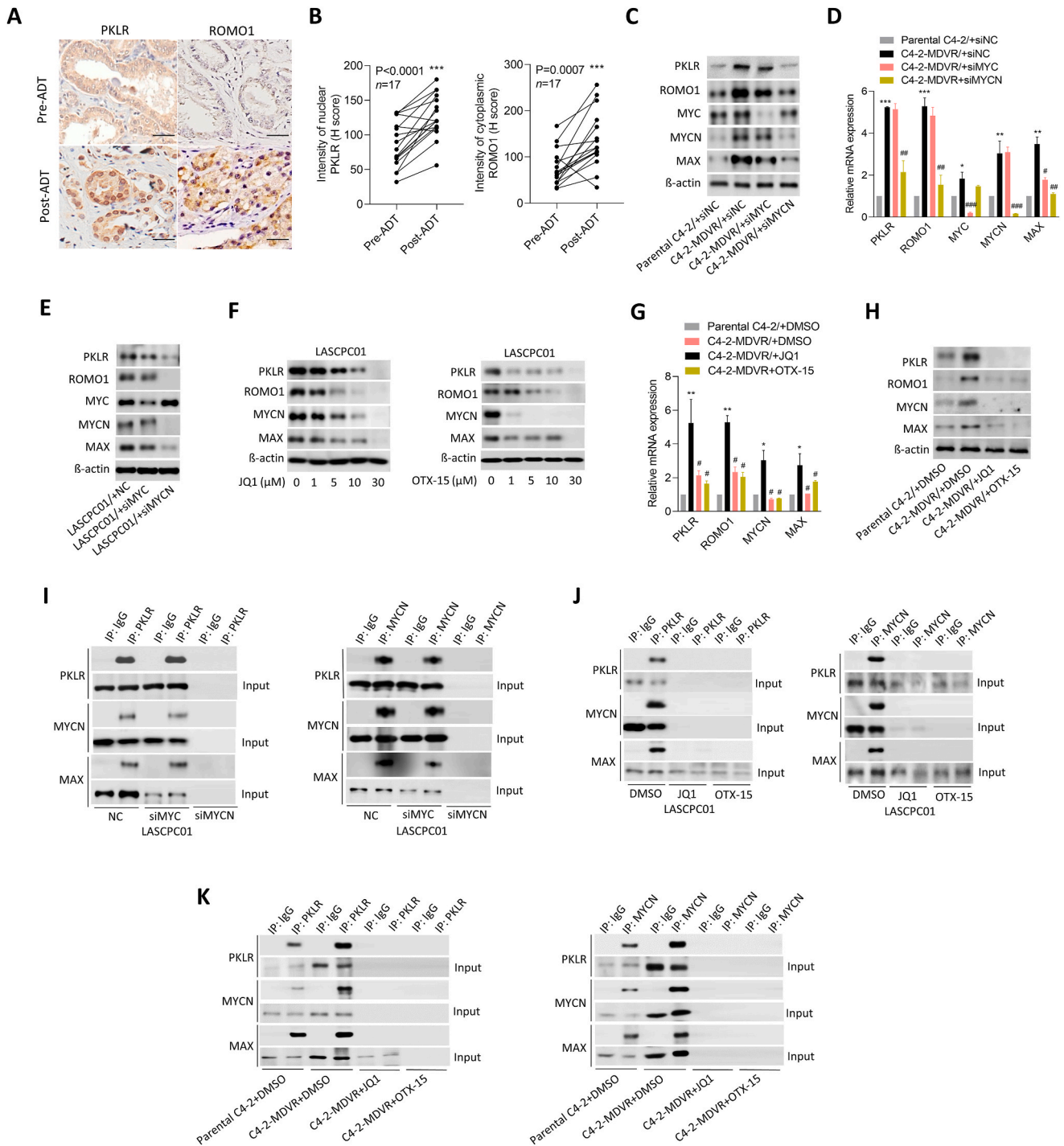


Fig. 5. Androgen-deprivation therapy (ADT) induces PKLR nuclear translocation where it may interact with the MYCN/MAX complex. (A and B) IHC staining and relative intensities of nuclear PKLR and cytoplasmic ROMO1 of prostate cancer (PCa) patients pre- and post-ADT treatment collected from Taipei Medical University-Wan Fang Hospital (Taipei, Taiwan). Scale bars represent 100 μm . $n = 17$. p values were calculated using a one-way ANOVA by correlation XY analyses in GraphPad Prism. (C and D) Relative protein (C) and mRNA (D) levels of PKLR, ROMO1, MYC, MYCN, and MAX in parental C4-2 or C4-2-MDVR cells transiently transfected with a non-targeting control (NC), or MYC or MYCN SMARTpool siRNA by WB (C) or an RT-qPCR (D). * vs. parental C4-2/+siNC cells; # vs. C4-2-MDVR/+siNC cells. (E) Relative protein levels of PKLR, ROMO1, MYC, MYCN, and MAX in LASCPC01 cells following transient transfection with the NC or MYC or MYCN SMARTpool siRNA by WB. (F) Protein levels of PKLR, ROMO1, MYCN, and MAX in LASCPC01 cells treated with 0, 1, 5, 10, and 30 μM of JQ1 (left) or OTX-15 (right) for 24 h by WB. (G and H) Relative mRNA (G) and protein (H) levels of PKLR, ROMO1, MYCN, and MAX in parental C4-2 or C4-2-MDVR cells treated with 30 μM JQ1 or 30 μM OTX-15 for 24 h by RT-qPCR (G) or WB (H). * vs. LNCaP/-CSS/+DMSO; # vs. LNCaP/+CSS/+DMSO. Data from relative mRNA levels are the mean \pm SEM of three independent experiments. * $p < 0.05$, ** $p < 0.01$, and *** $p < 0.001$ by a two-way ANOVA. (I) IP of IgG, PKLR (left), and MYCN (right) and WB of PKLR, MYCN, and MAX proteins in nuclear extracts of LASCPC01 cells transiently transfected with the NC or MYC or MYCN SMARTpool siRNA. (J) IP of IgG, PKLR (left), and MYCN (right) and WB of PKLR, MYCN, and MAX proteins in nuclear extracts of parental C4-2 cells or C4-2-MDVR cells treated with 30 μM JQ1 or 30 μM OTX-15 for 24 h.

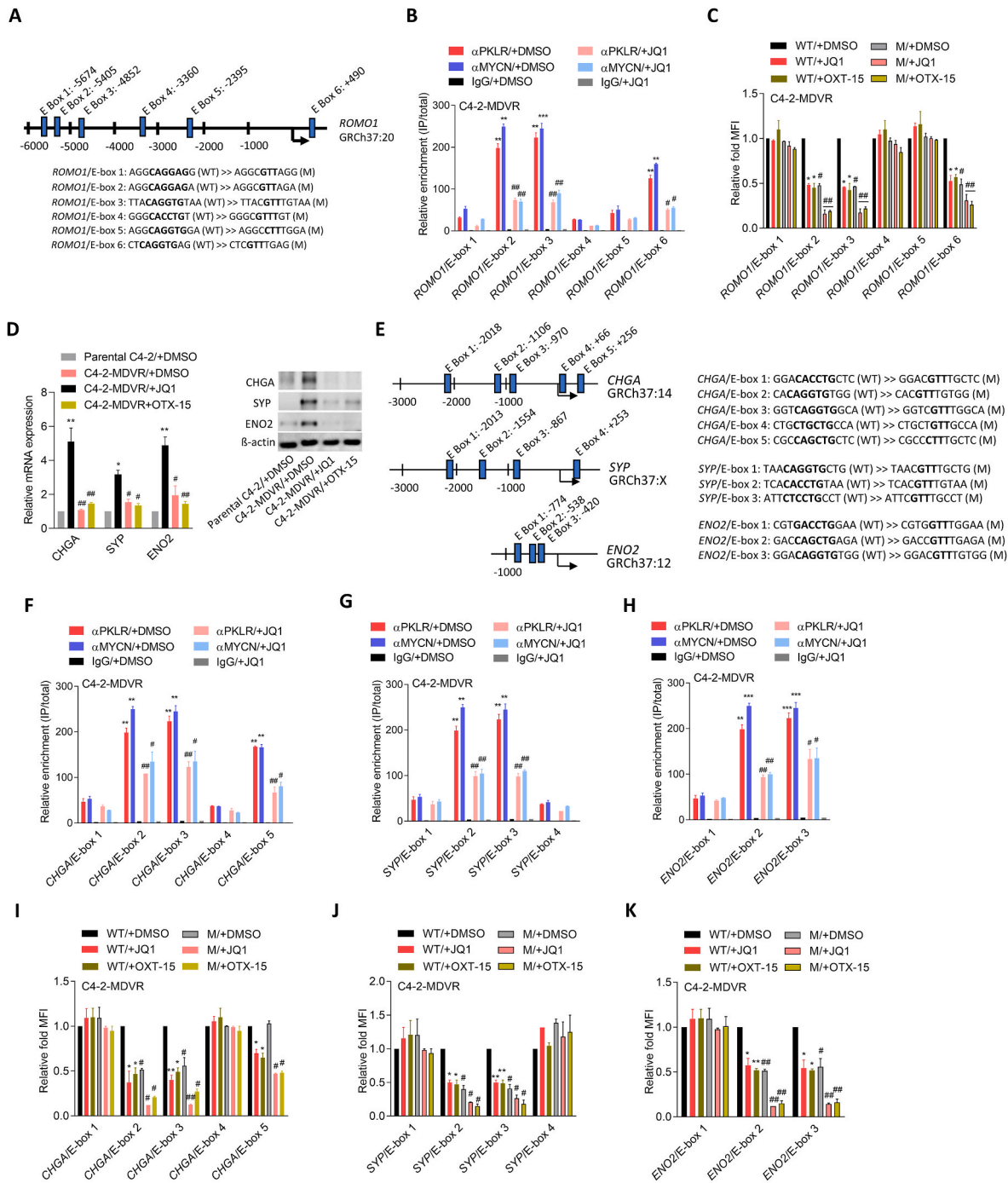


Fig. 6. The nuclear PKLR/MYCN complex may bind and activate regulatory sequences of *ROMO1*, *CHGA*, *SYP*, and *ENO2* in prostate cancer (PCa) cells after androgen-deprivation therapy (ADT).

(A) Schematic of the predicted E-box in the regulatory sequence of the human *ROMO1* gene (top). Wild-type (WT) and mutant (M) sequences of predicted E-boxes of the human *ROMO1* gene (bottom). (B) Chromatin immunoprecipitation (ChIP) assay showing binding of nuclear PKLR and MYCN to predicted E-boxes of *ROMO1* gene regulatory sequences following treatment of C4-2-MDVR cells with 30 μM JQ1 for 24 h. Sheared chromatin from nuclear extracts was precipitated with antibodies to PKLR and MYCN, and predictive primers for E-boxes (A) were used to quantify the precipitated DNA by a qPCR. Enrichment of each protein to each site is given as a percentage of the total input and then normalized to IgG. * vs. E-box 1; # vs. DMSO. (C) Promoter reporter assay of WT or M E-boxes in *ROMO1* gene regulatory sequences in parental C4-2 or C4-2-MDVR cells which were further treated with 30 μM JQ1 or 30 μM OTX-15 for 24 h * vs. DMSO; # vs. the WT. (D) Relative mRNA (left) and protein (right) levels of *CHGA*, *SYP*, and *ENO2* in parental C4-2 or C4-2-MDVR cells which were further treated with 30 μM JQ1 or 30 μM OTX-15 for 24 h by an RT-qPCR (left) or WB (right). * vs. parental C4-2; # vs. C4-2-MDVR/+DMSO. (E) Schematic of predicted E-boxes in the regulatory sequences of the human *CHGA*, *SYP*, and *ENO2* genes (left). WT and M sequences of predicted E-boxes of the human *CHGA*, *SYP*, and *ENO2* genes (right). (F–H) ChIP assay showing binding of nuclear PKLR and MYCN to regulatory sequences of the predicted E-boxes of *CHGA* (F), *SYP* (G), and *ENO2* (H) genes following treatment of C4-2-MDVR cells with 30 μM JQ1 or 30 μM OTX-15 for 24 h * vs. E-box 1; # vs. DMSO. (I–K) Promoter reporter assay of WT or M E-boxes of regulatory sequences of *CHGA* (I), *SYP* (J), and *ENO2* (K) genes in C4-2-MDVR cells following 30 μM JQ1 or 30 μM OTX-15 treatment for 24 h * vs. DMSO; # vs. the WT. Data from relative ChIP enrichment, mRNA levels, and mean fluorescent intensities (MFIs) of GFP are presented as the mean ± SEM of three independent experiments. **p* < 0.05, ***p* < 0.01, and ****p* < 0.001 by a two-way ANOVA.

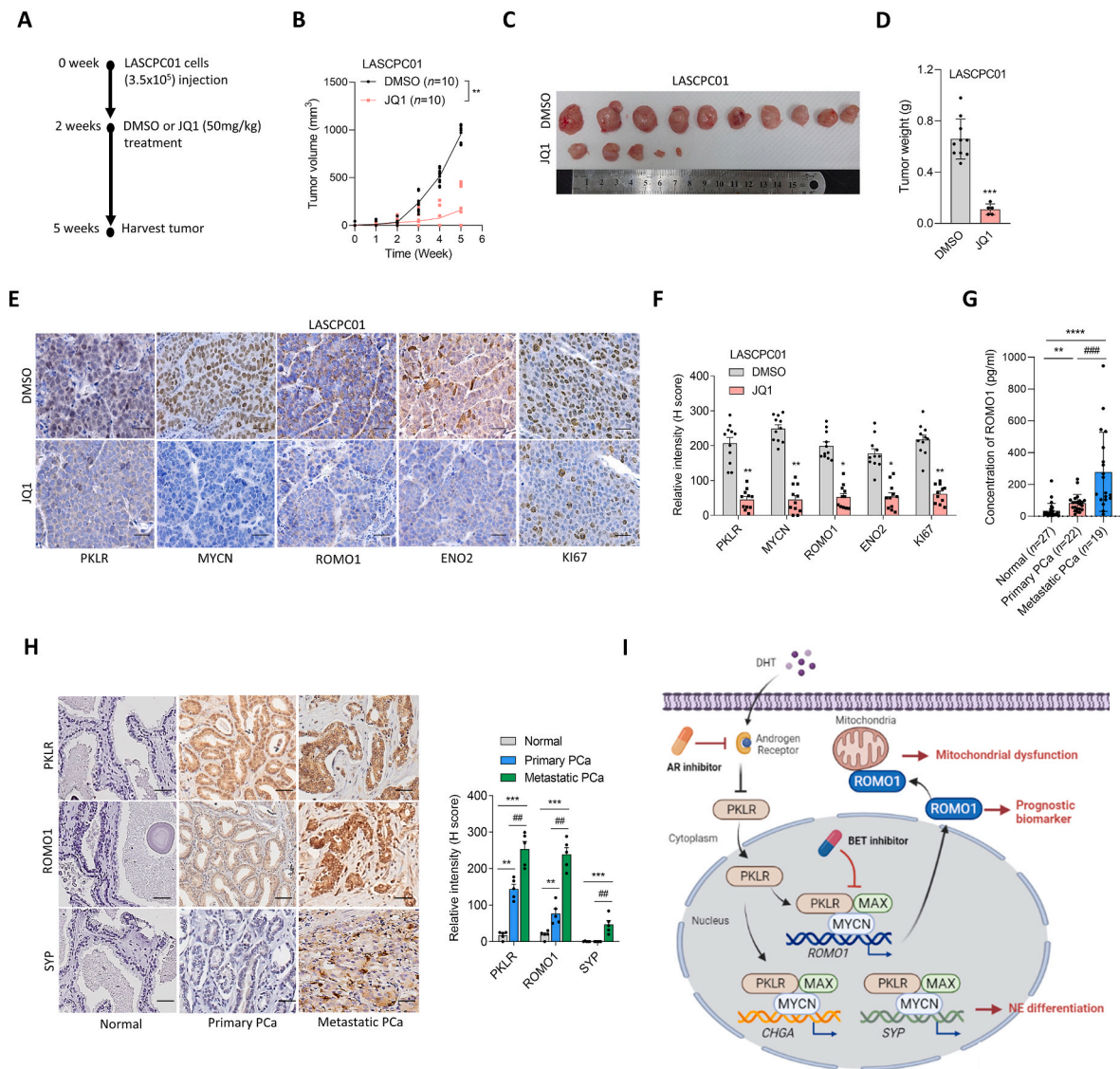


Fig. 7. PKLR/MYCN/ROMO1 is a potent therapeutic target for advanced neuroendocrine (NE)-like prostate cancer (PCa).

(A) Male nude mice subcutaneously injected with LASCPC01 cells were treated in a double-blinded manner with DMSO or JQ1 after 2 weeks of tumor formation, twice a week for a total of 5 weeks. (B–D) Analysis and images of subcutaneous tumor growth in mice inoculated with LASCPC01 cells and treated with DMSO or JQ1 (30 mg/kg). $n = 10$ /per group. The tumor volume (B) was monitored weekly, and images (C) and tumor weights (D) were obtained at the end of the experiment. * vs. DMSO. ** $p < 0.01$, and *** $p < 0.001$ by a one-way ANOVA. (E and F) IHC staining (E) and relative intensities (F) of PKLR, MYCN, ROMO1, ENO2, and Ki67 in subcutaneous tumors from (C). * vs. DMSO. * $p < 0.05$, ** $p < 0.01$, and *** $p < 0.001$ by a one-way ANOVA. Scale bars (E) represent 100 μm . (G) Concentration of ROMO1 in human serum from normal donors ($n = 27$), primary PCa patients ($n = 22$), and metastatic PCa patients ($n = 19$) collected from Taipei Medical University-Wan Fang Hospital. * vs. normal; # vs. primary PCa. (H) IHC staining of samples from normal, primary PCa patients, and metastatic PCa patients collected from (G) for PKLR, ROMO1, and SYP examination. Scale bars represent 100 μm . (I) Proposed model for ADT-induced nuclear translocation of PKLR which interacts with the MYCN/MAX complex and leads to increased abundance of ROMO1 and NE markers, resulting in altered mitochondrial function and NE differentiation in PCa.

the serum of patients with metastatic PCa, which correlated with increased expression of ROMO1 and NE markers in PCa tissues from the same patients, suggesting that serum ROMO1 measurements may be associated with metastasis or NED of PCa. Recent treatment of advanced PCa uses MDV3100 combined with radiotherapy or non-specific chemotherapeutic drugs, such as docetaxel or cabazitaxel, but this is unable to effectively eradicate NEPC progression [54]. Hence, identifying a promising targeted therapy for NEPC could improve the therapeutic efficacy and reduce the use of toxic chemotherapeutic regimens. Our study revealed the role of PKLR/MYCN/ROMO1 signaling in promoting NEPC progression and its contribution to mitochondrial dysfunction. We showed that targeting the nuclear PKLR/MYCN complex with BET inhibitors has the potential to be useful against ADT-resistant PCa and NEPC.

Alterations in glucose metabolism frequently occur during PCa progression and modulate intracellular ROS levels [14,15]. ROMO1 is a ROS sensor located in the inner membrane of mitochondria [31]. ROMO1 modulates tumor growth and metastasis by augmenting cytosolic ROS levels [55]. ROMO1 overexpression in various cancers, including non-small cell lung cancer, gastric cancer, gliomas, and colorectal cancer, was correlated with poor prognoses [39,56–58]. Although ROMO1 is considered a prognostic gene for PCa diagnosis and prognosis using bioinformatic analytical methods [59], the role and regulatory mechanisms of ROMO1 in mediating androgen-independent metabolic reprogramming of PCa remain unclear. Our study aimed to explore ADT-induced metabolic reprogramming of PCa and the impact of ROMO1 on the progression of therapy-induced NEPC. Our findings suggest that ADT increases the nuclear translocation of PKLR, which

interacts with MYCN/MAX and upregulates ROMO1-driven altered mitochondrial function associated with aggressive or NE-like features of PCa. We also found that ROMO1 abundance in serum was significantly associated with PKLR and NE marker expression in metastatic PCa patients compared to primary PCa or normal samples. This result suggests that ROMO1 serum abundance may be associated with the development of advanced NE-like PCa.

Alteration of mitochondrial function was proven to be an activator of resistance to AR antagonists and numerous chemotherapeutic drugs in PCa [14,15]. However, the mechanism underlying androgen-independent or NE-like PCa development caused by ADT-mediated oxidative stress remains unclear. Although upstream regulators of ROMO1, including Bcl-xL, DKK-1, and the long non-coding RNA, LINC00319, were demonstrated in bladder and lung cancer cells [60–62], the mechanism that promotes ROMO1 expression in PCa is unclear. Our study found significant correlations between ROMO1 and NE-related gene upregulation in PCa after ADT, which may have been caused by the nuclear translocation of PKLR and its interaction with the MYCN/MAX complex to promote ROMO1 and NE marker expression. Importantly, we found that this interaction decreased after treatment with a putative MYCN inhibitor. These data suggest that PKLR may also act as a transcription cofactor of MYCN, in addition to acting as a kinase, similar to PKM2, which acts as a transcription cofactor to activate hypoxia-inducible factor-1A (HIF1A) to promote castration resistance [22]. Our results showed that regulatory sequences of ROMO1, CHGA, SYP, and ENO2 genes have putative MYCN-responsive elements and illustrated the molecular mechanisms by which nuclear PKLR cross-talks with the MYCN/MAX pathway to upregulate ROMO1 and NE marker expression.

PKLR is a glycolytic enzyme that promotes the progression and metastasis of breast, colorectal, and pancreatic cancers [23,63,64]. Our recent study showed that loss of the androgen-responsive transcription factor, ZBTB10, may enhance PKLR upregulation [26]. We demonstrated that overexpression of ZBTB10 can suppress the expression and oncogenic effects of PKLR by directly binding to the PKLR regulatory sequence [26]. Herein, we showed a role for nuclear PKLR in PCa after ADT, and we verified that the nuclear PKLR-associated MYCN/MAX complex not only activates ROMO1-driven mitochondrial dysfunction, but also upregulates NE-related gene expression to promote NED progression. We provided evidence that ADT induces the accumulation of PKLR, which may act as a transcriptional coactivator of the nuclear MYCN/MAX complex to promote ROMO1 expression, thereby driving altered mitochondrial function in PCa cells. The MYC/MAX protein complex was shown to consist of multiple basic helix-loop-helix leucine zipper domain-containing regulators that induce translocation of transcriptional regulators from the nucleus to the cytoplasm following stress signals [44]. We hypothesized that the induction of AR-repressed transcriptional networks by the NED or ADT-resistant microenvironment in PCa cells might drive stress signals to enhance the accumulation of the MYCN/MAX/PKLR complex in the nucleus. Although ADT was shown to induce oxidative stress in PCa and trigger castration resistance [14,15], a missing link between ADT-induced nuclear translocation of PKLR and NEPC development still exists. The stress signals in PCa cells after ADT or NED progression that drive nuclear translocation of PKLR remain unclear.

NED is a highly complex process due to the heterogeneity of the prostate and the interplay between different factors in the development of NEPC [45]. The arising of basal cells to form *de novo* NEPC was proven by Lee et al. through lineage tracing experiments [65]. Interestingly ADT treatment is considered the driving factor inducing NEPC development in which inhibited AR signaling triggers clonal evolution of AR-independent NE and basal cells over AR-dependent subgroups [66]. The transdifferentiation of adenocarcinoma cells to NE cells is driven by different signaling molecules [7–10]. Upregulated NE markers (ENO2, CHGA, and SYP) are a sign of NED in PCa cells [45]. Our results demonstrated that stimulated PKLR levels associated with NE markers

were enriched in AR-negative PC3, NEPC-like LASCPC01, and MDV3100-resistant C4-2 cell lines. Upregulated PKLR is then translocated into the nucleus, where it may complex with MYCN and act as a transcription factor for ROMO1 and NE markers. Accumulating ROMO1 in PCa cells enhances mitochondrial dysfunction, thereby supporting cell viability in nutrient depletion of the tumor microenvironment. Increased PKLR upregulates expression of NE markers through the direct binding of the PKLR/MYCN complex to E-boxes of CHGA, SYP, and ENO2. Upregulation of PKLR/MYCN/ROMO1 signaling may play an important role in regulating the viability of NE-like cells and inducing NED in PCa.

Declaration of competing interest

The authors declare no competing interests.

Data availability

Data will be made available on request.

Acknowledgements

We thank Dr. Hsing-Jien Kung (Academician of Academia Sinica, Chair Professor of Taipei Medical University, Taiwan) for reading the manuscript and providing comments and helpful suggestions. We also thank Dr. Cheng-Wen Wu (Academician of Academia Sinica, Institute of Biomedical Sciences, Academia Sinica, Taiwan) and Dr. Shauh-Der Yeh (College of Medicine, Taipei Medical University, Taiwan) for their support and discussion on the experiments conducted in this study. This work was jointly supported by grants from the National Science and Technology Council, Taiwan (MOST109-2326-B-038-001-MY3 and MOST111-2628-B-038-016-MY3 to Y.N.L., and MOST111-2314-B-038-107-MY3 to Y.C.W.), National Health Research Institutes, Taiwan (NHRI-EX112-11109BI to Y.N.L.), and Wan Fang Hospital (111TMU-WFH-03 to W.Y.C.). This work was financially supported by the “TMU Research Center of Cancer Translational Medicine” from The Featured Areas Research Center Program within the framework of the Higher Education Sprout Project by the Ministry of Education (MOE) in Taiwan.

Appendix A. Supplementary data

Supplementary data to this article can be found online at <https://doi.org/10.1016/j.redox.2023.102686>.

References

- [1] R.L. Siegel, K.D. Miller, A. Jemal, Cancer statistics, 2020, CA, Cancer J. Clinic. 70 (1) (2020) 7–30.
- [2] J.E. Vellky, W.A. Ricke, Development and prevalence of castration-resistant prostate cancer subtypes, Neoplasia 22 (11) (2020) 566–575.
- [3] Q. Li, Q. Deng, H.-P. Chao, X. Liu, Y. Lu, K. Lin, B. Liu, G.W. Tang, D. Zhang, A. Tracz, C. Jeter, K. Rycaj, T. Calhoun-Davis, J. Huang, M.A. Rubin, H. Beltran, J. Shen, G. Chatta, I. Puzanov, J.L. Mohler, J. Wang, R. Zhao, J. Kirk, X. Chen, D. G. Tang, Linking prostate cancer cell AR heterogeneity to distinct castration and enzalutamide responses, Nat. Commun. 9 (1) (2018).
- [4] M. Nakazawa, C. Paller, N. Kyrianiou, Mechanisms of therapeutic resistance in prostate cancer, Curr. Oncol. Rep. 19 (2) (2017) 13.
- [5] C. Parker, E. Castro, K. Fizazi, A. Heidenreich, P. Ost, G. Procopio, B. Tombal, S. Gillissen, E.G.C.E.a. clinicalguidelines@esmo.org, Prostate cancer: ESMO Clinical Practice Guidelines for diagnosis, treatment and follow-up, Ann. Oncol. 31 (9) (2020) 1119–1134.
- [6] P.S. Nelson, N. Clegg, H. Arnold, C. Ferguson, M. Bonham, J. White, L. Hood, B. Lin, The program of androgen-responsive genes in neoplastic prostate epithelium, Proc. Natl. Acad. Sci. U. S. A. 99 (18) (2002) 11890–11895.
- [7] D. McKeithen, T. Graham, L.W. Chung, V. Odero-Marah, Snail transcription factor regulates neuroendocrine differentiation in LNCaP prostate cancer cells, Prostate 70 (9) (2010) 982–992.
- [8] M.E. Wright, M.J. Tsai, R. Aebbersold, Androgen receptor represses the neuroendocrine transdifferentiation process in prostate cancer cells, Mol. Endocrinol. 17 (9) (2003) 1726–1737.
- [9] G. Danza, C. Di Serio, F. Rosati, G. Lonetto, N. Sturli, D. Kacer, A. Pennella, G. Ventimiglia, R. Barucci, A. Piscazzi, I. Prudovsky, M. Landriscina,

- N. Marchionni, F. Tarantini, Notch signaling modulates hypoxia-induced neuroendocrine differentiation of human prostate cancer cells, *Mol. Cancer Res.* 10 (2) (2012) 230–238.
- [10] H. Liang, L. Studach, R.L. Hullinger, J. Xie, O.M. Andrisani, Down-regulation of RE-1 silencing transcription factor (REST) in advanced prostate cancer by hypoxia-induced miR-106b~25, *Exp. Cell Res.* 320 (2) (2014) 188–199.
- [11] B. Faubert, A. Solmonson, R.J. DeBerardinis, Metabolic reprogramming and cancer progression, *Science* 368 (6487) (2020).
- [12] S.S. Sabharwal, P.T. Schumacker, Mitochondrial ROS in cancer: initiators, amplifiers or an Achilles' heel? *Nat. Rev. Cancer* 14 (11) (2014) 709–721.
- [13] B. Kumar, S. Koul, L. Khandrika, R.B. Meacham, H.K. Koul, Oxidative stress is inherent in prostate cancer cells and is required for aggressive phenotype, *Cancer Res.* 68 (6) (2008) 1777–1785.
- [14] M. Shiota, A. Yokomizo, Y. Tada, J. Inokuchi, E. Kashiwagi, D. Masubuchi, M. Eto, T. Uchiyama, S. Naito, Castration resistance of prostate cancer cells caused by castration-induced oxidative stress through Twist1 and androgen receptor overexpression, *Oncogene* 29 (2) (2010) 237–250.
- [15] D.K. Price, Efficacy of androgen deprivation therapy and the role of oxidative stress, *Ann. Oncol.* 28 (3) (2017) 451–453.
- [16] J.P. Lu, L. Monardo, I. Bryskin, Z.F. Hou, J. Trachtenberg, B.C. Wilson, J. H. Pinthus, Androgens induce oxidative stress and radiation resistance in prostate cancer cells through NADPH oxidase, *Prostate Cancer Prostatic Dis.* 13 (1) (2010) 39–46.
- [17] M. Reina-Campos, J.F. Linares, A. Duran, T. Cordes, A. L'Hermitte, M.G. Badur, M. S. Bhangoo, P.K. Thorson, A. Richards, T. Rooslid, D.C. Garcia-Olmo, S.Y. Nam-Cha, A.S. Salinas-Sanchez, K. Eng, H. Beltran, D.A. Scott, C.M. Metallo, J. Moscat, M.T. Diaz-Meco, Increased serine and one-carbon pathway metabolism by PKC*lambda*/iota deficiency promotes neuroendocrine prostate cancer, *Cancer Cell* 35 (3) (2019) 385–400 e9.
- [18] F. Ahmad, M.K. Cherukuri, P.L. Choyke, Metabolic reprogramming in prostate cancer, *Br. J. Cancer* 125 (9) (2021) 1185–1196.
- [19] W.J. Israelsen, M.G. Vander Heiden, Pyruvate kinase: function, regulation and role in cancer, *Semin. Cell Dev. Biol.* 43 (2015) 43–51.
- [20] T.L. Dayton, T. Jacks, M.G. Vander Heiden, PKM2, cancer metabolism, and the road ahead, *EMBO Rep.* 17 (12) (2016) 1721–1730.
- [21] W. Yang, Y. Xia, H. Ji, Y. Zheng, J. Liang, W. Huang, X. Gao, K. Aldape, Z. Lu, Nuclear PKM2 regulates beta-catenin transactivation upon EGFR activation, *Nature* 480 (7375) (2011) 118–122.
- [22] D. Hasan, E. Gamem, N. Abu Tarboush, Y. Ismail, O. Pak, B. Azab, PKM2 and HIF-1alpha regulation in prostate cancer cell lines, *PLoS One* 13 (9) (2018), e0203745.
- [23] A. Nguyen, J.M. Loo, R. Mital, E.M. Weinberg, F.Y. Man, Z. Zeng, P.B. Paty, L. Saltz, Y.Y. Janjigian, E. de Stanchina, S.F. Tavazoie, PKLR promotes colorectal cancer liver colonization through induction of glutathione synthesis, *J. Clin. Invest.* 126 (2) (2016) 681–694.
- [24] K. Chella Krishnan, Z. Kurt, R. Barrere-Cain, S. Sabir, A. Das, R. Floyd, L. Vergnes, Y. Zhao, N. Che, S. Charugundia, H. Qi, Z. Zhou, Y. Meng, C. Pan, M.M. Seldin, F. Norheim, S. Hui, K. Reue, A.J. Lusis, X. Yang, Integration of multi-omics data from mouse diversity panel highlights mitochondrial dysfunction in non-alcoholic fatty liver disease, *Cell Syst.* 6 (1) (2018) 103–115 e7.
- [25] Z. Liu, C. Zhang, S. Lee, W. Kim, M. Kleivstig, A.M. Harzandi, N. Sikanic, M. Arif, M. Stahlman, J. Nielsen, M. Uhlen, J. Boren, A. Mardinoglu, Pyruvate kinase L/R is a regulator of lipid metabolism and mitochondrial function, *Metab. Eng.* 52 (2019) 263–272.
- [26] Y.C. Wen, W.Y. Chen, V.T.N. Tram, H.L. Yeh, W.H. Chen, K.C. Jiang, W. Abou-Kheir, J. Huang, M. Hsiao, Y.N. Liu, Pyruvate kinase L/R links metabolism dysfunction to neuroendocrine differentiation of prostate cancer by ZBTB10 deficiency, *Cell Death Dis.* 13 (3) (2022) 252.
- [27] T. Mizumachi, L. Muskhelishvili, A. Naito, J. Furusawa, C.Y. Fan, E.R. Siegel, F. F. Kadlubar, U. Kumar, M. Higuchi, Increased distributional variance of mitochondrial DNA content associated with prostate cancer cells as compared with normal prostate cells, *Prostate* 68 (4) (2008) 408–417.
- [28] K. Grupp, K. Jedrzejewska, M.C. Tsourlakis, C. Koop, W. Wilczak, M. Adam, A. Quaas, G. Sauter, R. Simon, J.R. Izbicki, M. Graefen, H. Huland, T. Schlomm, S. Minner, S. Steurer, High mitochondria content is associated with prostate cancer disease progression, *Mol. Cancer* 12 (1) (2013) 145.
- [29] M. Higuchi, T. Kudo, S. Suzuki, T.T. Evans, R. Sasaki, Y. Wada, T. Shirakawa, J. R. Sawyer, A. Gotoh, Mitochondrial DNA determines androgen dependence in prostate cancer cell lines, *Oncogene* 25 (10) (2006) 1437–1445.
- [30] L. Khandrika, B. Kumar, S. Koul, P. Maroni, H.K. Koul, Oxidative stress in prostate cancer, *Cancer Lett.* 282 (2) (2009) 125–136.
- [31] F. Richter, S. Dennerlein, M. Nikolov, D.C. Jans, N. Naumenko, A. Aich, T. MacVicar, A. Linden, S. Jakobs, H. Urlaub, T. Langer, P. Rehling, ROMO1 is a constituent of the human presequence translocase required for YME1L protease import, *J. Cell Biol.* 218 (2) (2019) 598–614.
- [32] M. Norton, A.C. Ng, S. Baird, A. Dumoulin, T. Shutt, N. Mah, M.A. Andrade-Navarro, H.M. McBride, R.A. Sreaton, ROMO1 is an essential redox-dependent regulator of mitochondrial dynamics, *Sci. Signal.* 7 (310) (2014) ra10.
- [33] J.M. Schafer, B.D. Lehmann, P.I. Gonzalez-Ericsson, C.B. Marshall, J.S. Beeler, L. N. Redman, H. Jin, V. Sanchez, M.C. Stubbs, P. Scherle, K.N. Johnson, Q. Sheng, J. T. Roland, J.A. Bauer, Y. Shyr, B. Chakravarthy, B.C. Mobley, S.W. Hiebert, J. M. Balko, M.E. Sanders, P.C.C. Liu, J.A. Pietenpol, Targeting MYCN-expressing triple-negative breast cancer with BET and MEK inhibitors, *Sci. Transl. Med.* 12 (534) (2020).
- [34] C. Berthon, E. Raffoux, X. Thomas, N. Vey, C. Gomez-Roca, K. Yee, D.C. Taussig, K. Rezaei, C. Roumier, P. Herait, C. Kahatt, B. Quesnel, M. Michallet, C. Recher, F. Lokiec, C. Preudhomme, H. Dombret, Bromodomain inhibitor OTX015 in patients with acute leukaemia: a dose-escalation, phase 1 study, *Lancet Haematol.* 3 (4) (2016) e186–e195.
- [35] S.R. Lin, Y.C. Wen, H.L. Yeh, K.C. Jiang, W.H. Chen, N. Moksauts, J. Huang, W. Y. Chen, Y.N. Liu, EGFR-upregulated LIFR promotes SUCLG2-dependent castration resistance and neuroendocrine differentiation of prostate cancer, *Oncogene* 39 (44) (2020) 6757–6775.
- [36] B.S. Taylor, N. Schultz, H. Hieronymus, A. Gopalan, Y. Xiao, B.S. Carver, V. K. Arora, P. Kaushik, E. Cerami, B. Reva, Y. Antipin, N. Mitsiades, T. Landers, I. Dolgalev, J.E. Major, M. Wilson, N.D. Socci, A.E. Lash, A. Heguy, J.A. Eastham, H.I. Scher, V.E. Reuter, P.T. Scardino, C. Sander, C.L. Sawyers, W.L. Gerald, Integrative genomic profiling of human prostate cancer, *Cancer Cell* 18 (1) (2010) 11–22.
- [37] T. Kim, Y.J. Cha, J.H. Park, A. Kim, Y.J. Choi, H.J. Park, Reactive oxygen species modulator 1 expression predicts lymph node metastasis and survival in early-stage non-small cell lung cancer, *PLoS One* 15 (12) (2020), e0239670.
- [38] H. Ghasemi, M.A. Amini, A. Pegah, E. Azizi, H. Tayebinia, S. Khanverdilu, S. H. Mousavibahar, A. Alizamir, Overexpression of reactive oxygen species modulator 1 is associated with advanced grades of bladder cancer, *Mol. Biol. Rep.* 47 (9) (2020) 6497–6505.
- [39] H.J. Kim, M.J. Jo, B.R. Kim, J.L. Kim, Y.A. Jeong, Y.J. Na, S.H. Park, S.Y. Lee, D. H. Lee, H.S. Lee, B.H. Kim, S.I. Lee, B.W. Min, Y.D. Yoo, S.C. Oh, Reactive oxygen species modulator-1 (Romol1) predicts unfavorable prognosis in colorectal cancer patients, *PLoS One* 12 (5) (2017), e0176834.
- [40] Y. Sun, J. Niu, J. Huang, Neuroendocrine differentiation in prostate cancer, *Am. J. Transl. Res.* 1 (2) (2009) 148–162.
- [41] J.K. Lee, J.W. Phillips, B.A. Smith, J.W. Park, T. Stoyanova, E.F. McCaffrey, R. Baertsch, A. Sokolov, J.G. Meyerowitz, C. Mathis, D. Cheng, J.M. Stuart, K. M. Shokat, W.C. Gustafson, J. Huang, O.N. Witte, N-myc drives neuroendocrine prostate cancer initiated from human prostate epithelial cells, *Cancer Cell* 29 (4) (2016) 536–547.
- [42] M.J. Sikora, M.D. Johnson, A.V. Lee, S. Oesterreich, Endocrine response phenotypes are altered by charcoal-stripped serum variability, *Endocrinology* 157 (10) (2016) 3760–3766.
- [43] C. Wang, G. Peng, H. Huang, F. Liu, D.P. Kong, K.Q. Dong, L.H. Dai, Z. Zhou, K. J. Wang, J. Yang, Y.Q. Cheng, X. Gao, M. Qu, H.R. Wang, F. Zhu, Q.Q. Tian, D. Liu, L. Cao, X.G. Cui, C.L. Xu, D.F. Xu, Y.H. Sun, Blocking the feedback loop between neuroendocrine differentiation and macrophages improves the therapeutic effects of enzalutamide (MDV3100) on prostate cancer, *Clin. Cancer Res.* 24 (3) (2018) 708–723.
- [44] Y. Kong, L. Cheng, F. Mao, Z. Zhang, Y. Zhang, E. Farah, J. Bosler, Y. Bai, N. Ahmad, S. Kuang, L. Li, X. Liu, Inhibition of cholesterol biosynthesis overcomes enzalutamide resistance in castration-resistant prostate cancer (CRPC), *J. Biol. Chem.* 293 (37) (2018) 14328–14341.
- [45] H. Beltran, D. Prandi, J.M. Mosquera, M. Benelli, L. Puca, J. Cyrta, C. Marozz, E. Giannopoulou, B.V. Chakravarthy, S. Varambally, S.A. Tomlins, D.M. Nanus, S. T. Tagawa, E.M. Van Allen, O. Elemento, A. Sboner, L.A. Garraway, M.A. Rubin, F. Demicheli, Divergent clonal evolution of castration-resistant neuroendocrine prostate cancer, *Nat. Med.* 22 (3) (2016) 298–305.
- [46] G. Wang, S.J. Jones, M.A. Marra, M.D. Sadar, Identification of genes targeted by the androgen and PKA signaling pathways in prostate cancer cells, *Oncogene* 25 (55) (2006) 7311–7323.
- [47] A.S. Doane, M. Danso, P. Lal, M. Donaton, L. Zhang, C. Hudis, W.L. Gerald, An estrogen receptor-negative breast cancer subset characterized by a hormonally regulated transcriptional program and response to androgen, *Oncogene* 25 (28) (2006) 3994–4008.
- [48] M. Eilers, R.N. Eisenman, Myc's broad reach, *Genes Dev.* 22 (20) (2008) 2755–2766.
- [49] S. He, Z. Liu, D.Y. Oh, C.J. Thiele, MYCN and the epigenome, *Front. Oncol.* 3 (2013) 1.
- [50] A. Berger, N.J. Brady, R. Bareja, B. Robinson, V. Conteduca, M.A. Augello, L. Puca, A. Ahmed, E. Dardenne, X. Lu, I. Hwang, A.M. Bagadion, A. Sboner, O. Elemento, J. Paik, J. Yu, C.E. Barbieri, N. Dephore, H. Beltran, D.S. Rickman, N-Myc-mediated epigenetic reprogramming drives lineage plasticity in advanced prostate cancer, *J. Clin. Invest.* 129 (9) (2019) 3924–3940.
- [51] R. Zeid, M.A. Lawlor, E. Poon, J.M. Reyes, M. Fulciniti, M.A. Lopez, T.G. Scott, B. Baret, M.A. Erb, G.E. Winter, Z. Jacobson, D.R. Polaski, K.L. Karlin, R.A. Hirsch, N.P. Munshi, T.F. Westbrook, L. Chesler, C.Y. Lin, J.E. Bradner, Enhancer invasion shapes MYCN-dependent transcriptional amplification in neuroblastoma, *Nat. Genet.* 50 (4) (2018) 515–523.
- [52] S. Gkolfinopoulos, K. Tsapakidis, K. Papadimitriou, D. Papamichael, P. Kountourakis, Chromogranin A as a valid marker in oncology: clinical application or false hopes? *World J. Methodol.* 7 (1) (2017) 9–15.
- [53] S.H. Lee, J.S. Lee, E.J. Lee, K.H. Min, G.Y. Hur, S.H. Lee, S.Y. Lee, J.H. Kim, S. Y. Lee, C. Shin, J.J. Shim, K.H. Kang, K. H. In, Serum reactive oxygen species modulator 1 (Romol1) as a potential diagnostic biomarker for non-small cell lung cancer, *Lung Cancer* 85 (2) (2014) 175–181.
- [54] W.T. Lowrance, M.H. Murad, W.K. Oh, D.F. Jarrard, M.J. Resnick, M.S. Cookson, Castration-resistant prostate cancer: AUA guideline amendment 2018, *J. Urol.* 200 (6) (2018) 1264–1272.
- [55] Y.M. Chung, J.S. Kim, Y.D. Yoo, A novel protein, Romol1, induces ROS production in the mitochondria, *Biochem. Biophys. Res. Commun.* 347 (3) (2006) 649–655.
- [56] H.J. Kim, M.J. Jo, B.R. Kim, J.L. Kim, Y.A. Jeong, Y.J. Na, S.H. Park, S.Y. Lee, D. H. Lee, B.H. Kim, Y.D. Yoo, S.C. Oh, Overexpression of Romol1 is an unfavorable prognostic biomarker and a predictor of lymphatic metastasis in non-small cell lung cancer patients, *OncoTargets Ther.* 11 (2018) 4233–4246.

- [57] M.A. Amini, J. Karimi, I. Khodadadi, H. Tavilani, S.S. Talebi, B. Afshar, Overexpression of ROMO1 and OMA1 are potentially biomarkers and predict unfavorable prognosis in gastric cancer, *J. Gastrointest. Cancer* 51 (3) (2020) 939–946.
- [58] M.O. Yu, N.H. Song, K.J. Park, D.H. Park, S.H. Kim, Y.S. Chae, Y.G. Chung, S. G. Chi, S.H. Kang, Romo1 is associated with ROS production and cellular growth in human gliomas, *J. Neuro Oncol.* 121 (1) (2015) 73–81.
- [59] L. Wang, X. Liu, Z. Liu, Y. Wang, M. Fan, J. Yin, Y. Zhang, Y. Ma, J. Luo, R. Li, X. Zhao, P. Zhang, L. Zhao, J. Fan, Y. Chen, W. Lu, X. Song, Network models of prostate cancer immune microenvironments identify ROMO1 as heterogeneity and prognostic marker, *Sci. Rep.* 12 (1) (2022) 192.
- [60] Y. Yang, F. Zhang, H. Huang, Z. Xie, W. Huang, H. Xie, F. Wang, Long noncoding RNA LINC00319 regulates ROMO1 expression and promotes bladder cancer progression via miR-4492/ROMO1 axis, *J. Cell. Physiol.* 235 (4) (2020) 3768–3775.
- [61] I.G. Kim, S.Y. Kim, H.A. Kim, J.Y. Kim, J.H. Lee, S.I. Choi, J.R. Han, K.C. Kim, E. W. Cho, Disturbance of DKK1 level is partly involved in survival of lung cancer cells via regulation of ROMO1 and gamma-radiation sensitivity, *Biochem. Biophys. Res. Commun.* 443 (1) (2014) 49–55.
- [62] S.B. Lee, H.J. Kim, J. Shin, S.T. Kang, S. Kang, Y.D. Yoo, Bcl-XL prevents serum deprivation-induced oxidative stress mediated by Romo1, *Oncol. Rep.* 25 (5) (2011) 1337–1342.
- [63] Y. Yang, G. Zhu, B. Dong, J. Piao, L. Chen, Z. Lin, The NQO1/PKLR axis promotes lymph node metastasis and breast cancer progression by modulating glycolytic reprogramming, *Cancer Lett.* 453 (2019) 170–183.
- [64] Z. Fan, K. Fan, S. Deng, Y. Gong, Y. Qian, Q. Huang, C. Yang, H. Cheng, K. Jin, G. Luo, C. Liu, X. Yu, HNF-1a promotes pancreatic cancer growth and apoptosis resistance via its target gene PKLR, *Acta Biochim. Biophys. Sin.* 52 (3) (2020) 241–250.
- [65] D.K. Lee, Y. Liu, L. Liao, W. Li, D. Danielpour, J. Xu, Neuroendocrine prostate carcinoma cells originate from the p63-expressing basal cells but not the pre-existing adenocarcinoma cells in mice, *Cell Res.* 29 (5) (2019) 420–422.
- [66] J.I. Epstein, M.B. Amin, H. Beltran, T.L. Lotan, J.M. Mosquera, V.E. Reuter, B. D. Robinson, P. Troncoso, M.A. Rubin, Proposed morphologic classification of prostate cancer with neuroendocrine differentiation, *Am. J. Surg. Pathol.* 38 (6) (2014) 756–767.